A review of current collectors for lithium-ion batteries

Zhu, Pengcheng; Gastol, Dominika; Marshall, Jean; Sommerville, Roberto; Goodship, Vannessa; Kendrick, Emma

DOI:
10.1016/j.jpowsour.2020.229321

Document Version
Peer reviewed version

Citation for published version (Harvard):
Zhu, P, Gastol, D, Marshall, J, Sommerville, R, Goodship, V & Kendrick, E 2021, 'A review of current collectors for lithium-ion batteries', *Journal of Power Sources*, vol. 485, 229321.
https://doi.org/10.1016/j.jpowsour.2020.229321

A review of current collectors for Lithium-ion batteries

Pengcheng Zhu[a], **Dominika Gastol**[b], **Jean Marshall**[a], **Roberto Sommerville**[b], **Vannessa Goodship**[a], **Emma Kendrick**[b, *]

[a]*WMG, University of Warwick, Coventry, CV4 7AL, United Kingdom*

[b]*School of Metallurgy and Materials, University of Birmingham, Edgbaston, Birmingham B15 2TT, United Kingdom*

∗Corresponding author

E.Kendrick@bham.ac.uk (Professor Emma Kendrick)

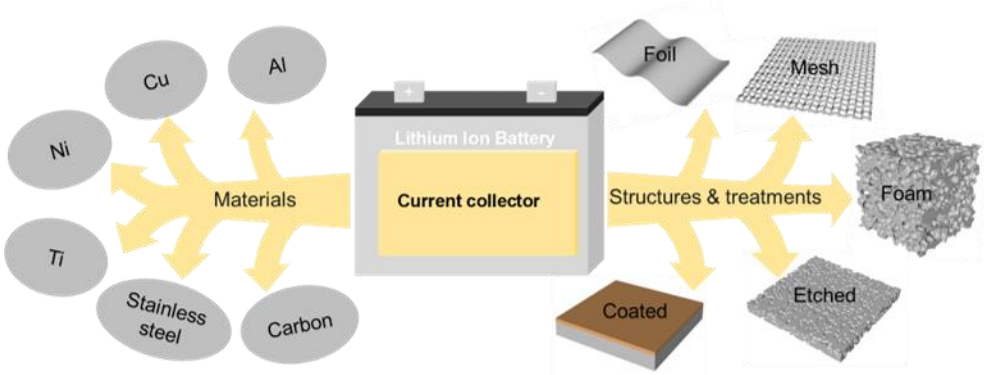

Abstract

Lithium-ion batteries are the state-of-the-art power source for most consumer electronic devices. Current collectors are indispensable components bridging lithium-ion batteries and external circuits, greatly influencing the capacity, rate capability and long-term stability of lithium-ion batteries. Conventional current collectors, Al and Cu foils have been used since the first commercial lithium-ion battery, and over the past two decades, the thickness of these current collectors has decreased in order to increase the energy density. However to improve the performance further, alternative materials and structures, as well as specific treatments such as etching and carbon coating, have also been investigated to enhance the electrochemical stability and electrical conductivity of current collectors, for next-generation lithium-ion batteries with higher capacities and longer service lifetime. This work reviews six types of materials for current collectors, including Al, Cu, Ni, Ti, stainless steel and

carbonaceous materials, and compares these materials from five aspects of electrochemical stability, electrical conductivity, mechanical property, density and sustainability. The effects of three different structures of foil, mesh and foam as well as two treatments of chemical etching and coating are also discussed. Future opportunities are highlighted at the end of this review.

Keywords: Current collector, lithium-ion battery, metal, carbonaceous material

Highlights:

- Six different types of current collector materials for batteries are reviewed
- The performance, stability, cost and sustainability are compared
- 2D and 3D structures of foil, mesh and foam are introduced
- Future direction and opportunities for 2D and 3D current collectors are provided

1. Introduction

The Lithium-ion battery (LIB) is currently the most commercially successful power storage and generation device due to its comprehensive superiority in power density, energy density, cost and safety [1]. LIBs store electricity in chemicals and convert chemical energy into electricity via electrochemical reactions, which have been regarded as a clean source of energy [2]. Their high energy and power densities enable LIBs to power not only portable devices, e.g. phones, tablets and laptops, but also electric vehicles, effectively reducing the consumption of fossil fuels and greenhouse gas emission [3-5]. Furthermore, the high energy conversion rate of LIBs enables them to be employed in electrical grid applications, allowing efficient storage of energy harvested from renewable sources, e.g. wind, solar and geothermal [6]. It is predicted that LIBs will continue to play an omnipresent role in our daily life.

A typical LIB is composed of a cathode, an anode, a separator, electrolyte and two current collectors, as shown in Fig. 1a. Commonly used cathodes include $LiCoO_2$, (LCO) $LiMn_2O_4$ (LMO), $LiFePO_4$ (LFP), and $LiNiMnCoO_2$ (NMC) and the anode mainly used is graphite [7, 8], which more recently contains additional active components such as SiO_x to improve the capacity [9]. During discharging, Li-ions stored at the anode move to the cathode, generating electrons and forming current flow. The process is reversed when the battery is being charged. Electrolytes consist of lithium salts, e.g. $LiPF_6$, $LiBF_4$, $LiClO_4$, in some organic solvents, e.g. propylene carbonate (PC), ethylene carbonate (EC), ethyl methyl carbonate (EMC), dimethyl carbonate (DMC), diethyl carbonate (DEC), that act as the conductive pathway for Li-ions movement [10]. Separators, normally microporous layers consisting of either polymeric membranes or non-woven fabric mats, are placed between the cathode and anode to prevent physical contact [11]. Current collectors are bridging components that collect electrical current generated at the electrodes and connect with external circuits. Commercial current collectors are Al and Cu foils for cathodes and anodes, respectively [12].

In 1998, Johnson and White systematically characterised some commercial LIBs produced by five dominant manufacturers [13], including Sony, Moli Energy, A & T Battery, Sanyo Electric and Matsushita Electric Industrial. Taking the average value from the five manufacturers, the weight percentages of cathode, anode, Al foil, Cu foil,

separator and other components are 29%, 13%, 5%, 13%, 5% and 35%, respectively. Fig. 1b shows the weight percentages of the main components in more recent LIBs [14]. The cathode and anode together make up the highest proportion, 40% of the total weight of LIBs. The two current collectors occupy the second-highest proportion with a percentage of 15%, the electrolyte accounts for 11% and separator has the lowest weight percentage of 4%. Other components, including case and tab, make up 30% of the total weight. One observation is that the weight percentages of the current collectors in LIBs has reduced slightly from 18% to 15% over the past two decades.

Current collectors can greatly influence the performance of LIBs. For example, improving the electrical conductivity, reducing contact resistance and increasing the corrosion resistance of current collectors are beneficial to increase the capacity, rate capability, efficiency and cycle stability of LIBs [15]. Considering current collectors are essentially non-active materials in LIBs, reducing the thickness of current collectors can reduce the weight percentage and thus increase the energy density of LIBs. Recent research pointed out that the thicknesses of Al and Cu current collectors are reduced down to 10 μm for the pursuit of high energy density [16]. Nevertheless, thin current collectors will sacrifice the electrical conductivity and heat transfer property of current collectors and in turn power density. Therefore, there is a trade-off between power and energy of LIBs in the design of these current collectors. Furthermore, as electrodes are adhered to current collectors, mechanical integrity is also required in current collectors in order to maintain a suitable bond to the electrodes during battery cycling, this adhesive strength also contributes to the internal contact resistance of the cell, and requires minimisation. More importantly, current collectors are indispensable components for the present LIBs, any improvements in current collectors are expected to benefit all LIBs. Fig. 1c displays a brief timeline of the development of current collectors for LIBs in both industry and academia over the past three decades.

Many efforts have been made in reviewing cathodes, anodes, electrolytes and separators of LIBs. However, to our knowledge, few reviews on current collectors have so far been published and these only review limited materials or structures [17, 18]. This brings us to the need for a more comprehensive review of current collectors. This paper attempts to review the development of various current collectors for LIBs in the literature, including Al, Cu, Ni, Ti, stainless steel and carbonaceous materials. For Al and Cu current collectors, we have further classified them into different categories

according to structures and treatments, namely foil, mesh, foam, etched and coated current collectors. Research challenges and future directions for current collectors are discussed at the end of this review.

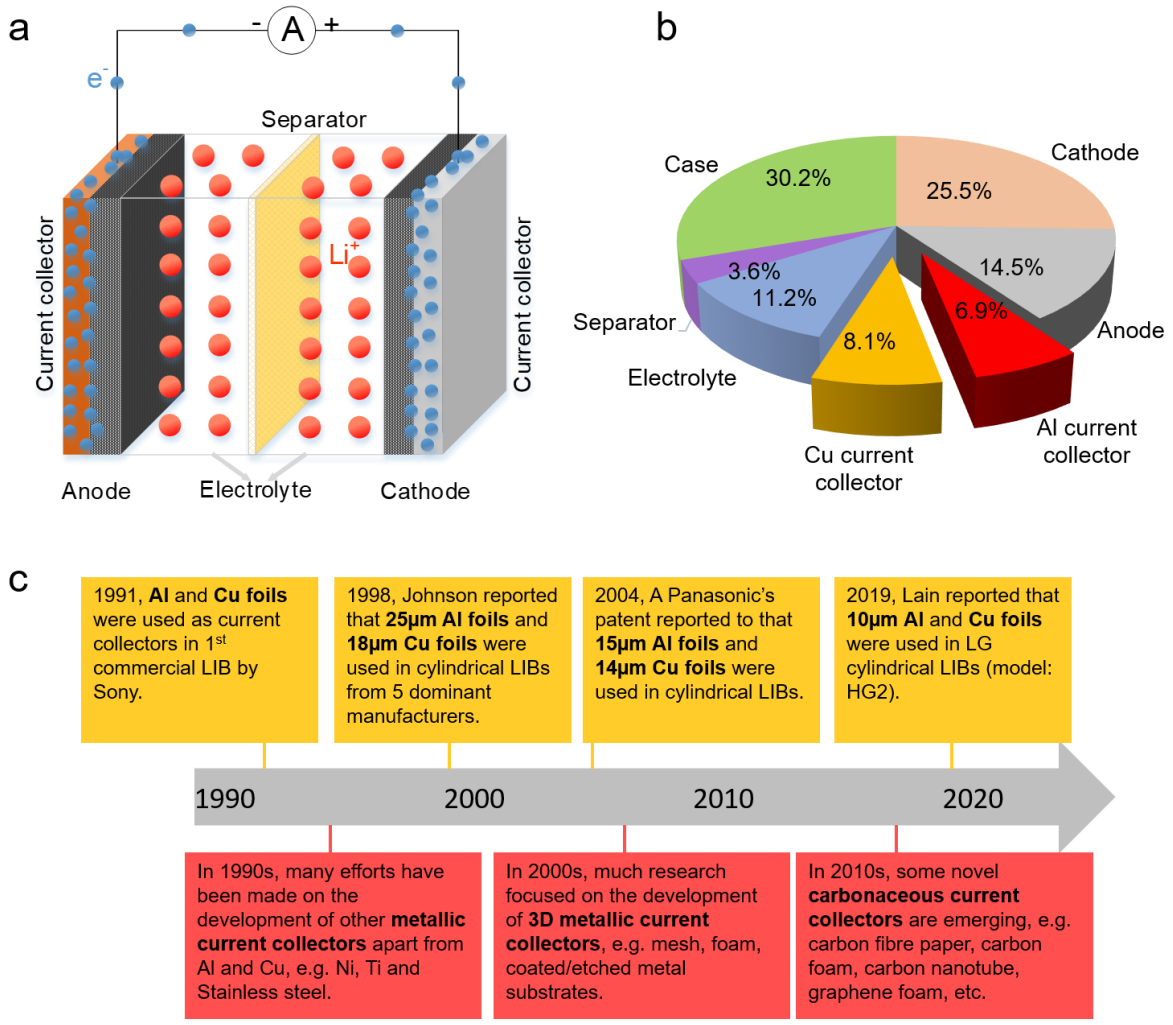

Fig. 1 a) Schematic diagram of a typical Li-ion battery, b) the weight percentage of main components in LIBs [14], c) historical timeline of the development of current collectors for LIBs in both industry (yellow) and academia (red) [13, 16, 19, 20].

2. Main requirements for current collectors in lithium-ion batteries

a) Electrochemical stability. Current collectors must be electrochemically stable against oxidation and reduction environments during battery charging and discharging. In practice, a high voltage is favourable for increasing battery energy density, which requires that cathodes and anodes have high and low electrochemical potentials, respectively, e.g. $LiCoO_2$ cathode(~4 V vs Li/Li^+) [21],

$LiFePO_4$ cathode (3.45 V vs Li/Li^+) [22], and graphite anode (0.01 – 0.25 V vs Li/Li^+) [23]. However, it is challenging to keep current collectors stable when in direct contact with electrolytes at such high and low potentials. Any undesired reactions of current collectors may cause serious capacity fading and short service lifetimes [24]. Therefore, good electrochemical stability is a prerequisite for all current collectors. In this review, the electrochemical stability will be discussed first in each section.

b) Electrical conductivity. All LIBs benefit from high electrical conductivity of current collectors [25]. During battery cycling, electrons generated at the electrodes travel through current collectors to external circuits. It is not only the conductivity of current collectors that is crucial for LIB performance but also the electrode/current collector interfacial conductivity. High electrical conductivity leads to low transformation of chemical/electrical energy into heat during discharging/charging process, contributing to high energy efficiency and capacity as well as avoiding the risk of high temperatures.

c) Mechanical strength. Commercial electrodes in LIBs are fabricated by slurry casting on metal foil current collectors [26]. The current collector serves as a mechanical support for the electrode. Polymeric binder, usually polyvinylidene difluoride (PVDF), is used to improve the integrity of the electrodes and adhesion between electrodes and current collectors. Some electrodes undergo significant volume change during cycling, which may cause serious electrode pulverisation or delamination, particularly for thick electrodes. A typical example is Si anode which suffers from up to 400% volume expansion due to the formation of LiSi alloy [27]. Current collectors with suitable levels of mechanical strength are helpful to maintain the bonding of electrode active materials to the current collector and the integrity of the whole electrodes during cycling.

d) Density. Conventional current collectors are non-active materials in LIBs as they do not participate in electrochemical reactions during cycling. However, the current collectors account for up to 20% of the total weight of LIBs. Using current collectors with low densities is therefore favourable for reducing the overall weight of LIBs and increasing the specific energy density of LIBs [28].

e) Sustainability and cost. The sustainable use of materials, in particular the critical elements and strategic materials is crucial for the future of the battery industry. The circular economic picture of cost, global availability and recyclability need to be

taken into consideration when we select and utilise materials for future current collectors. Although cost is one of the most important concerns for commercialization, what happens to the materials at end of the devices lide also needs consideration. The cost of current collectors may be reduced and the circular economy of battery technologies improved by recycling current collectors from end-of-life LIBs [29].

3. Materials for current collectors

3.1 Al

3.1.1 Electrochemical stability

The electrochemical behaviour of Al in the electrolyte of $LiPF_6$ in EC:DMC (1:1 vol.%) was reported by Myung et al. [30], as shown in Fig. 2a. A cathodic peak at 0 V vs Li/Li^+ and an anodic peak at 0.6 V vs Li/Li^+ represent the alloying reaction between Al and Li as well as the subsequent dealloying process, respectively. Two small anodic peaks at about 3.7 and 4.7 V vs Li/Li^+ result from the formation of a passivation film on Al surface. Similar electrochemical behaviour of Al was reported previously [31]. The current remains at about 0 mA cm^{-2} as the potential moves to 5 V vs Li/Li^+, indicating good electrochemical stability. The good electrochemical stability is attributed to a passivation film on Al surface, which consists of Al_2O_3 and AlF_3. The structure of this passivation film was identified by Zhang and Devine [32]. As shown in Fig. 2b, the passivation film consists of an air-formed Al_2O_3 layer with a thickness of 1.2 – 2.4 nm on the bottom and a thin layer of AlF_3 with an estimated thickness of 1 nm on the top. Myung et al. proposed a possible mechanism of the formation of AlF_3 [30]. As shown in Eqs. 1 – 3, AlF_3 is derived from the reaction between Al_2O_3 and HF which is generated from the decomposition of $LiPF_6$. Some factors, e.g. elevated temperature, high potential and addition of H_2O, can facilitate the decomposition of $LiPF_6$, boosting the formation of the AlF_3 passivation layer [33, 34],

$$Al_2O_3 + 2HF \rightarrow 2AlOF + H_2O \quad \text{Eq. 1}$$

$$2AlOF + 2HF \rightarrow Al_2OF_4 + H_2O \quad \text{Eq. 2}$$

$$Al_2OF_4 + 2HF \rightarrow 2AlF_3 + H_2O \quad \text{Eq. 3}$$

The reactions stop when the AlF_3 passivation film is formed completely.[35]. The electrochemical stability of Al is sensitive to both lithium salts and solvents. Similar to

$LiPF_6$, $LiB(C_2O_4)_2$ is another lithium salt which allows Al to form a passivation film of $AlBO_3$ against corrosion [36]. Though Al shows excellent corrosion resistance in electrolytes containing $LiPF_6$ and $LiB(C_2O_4)_2$, it is not stable in electrolytes containing many other lithium salts, e.g. $LiN(CF_3SO_2)_2$, $LiC(CF_3SO_2)_3$, $LiCF_3SO_3$, and $LiClO_4$, because the Al surface is only partially covered with AlF_3 [37, 38]. To this end, an effective strategy is to use $LiPF_6$, $LiBF_4$, $LiB(C_2O_4)_2$, or $LiBF_2(C_2O_4)$, as additives in electrolytes to allow the formation of passivation films on the Al surface [39-43]. In addition to lithium salts, solvents also have an effect upon the electrochemical stability of Al, this is known to be related to their dielectric constant [44]. Solvents with low dielectric constants are favourable, these exhibit limited solubility of the corrosion products, instead of forming a protective layer adhered to the Al surface. Solvents with high dielectric constants easily solvate the corrosion products removing them from the current collector surface, diffusing into the bulk electrolyte. An example is using methyl difluoroacetate (MFA) to replace EC:DMC (1:1 vol.%), which can improve the electrochemical stability of Al current collectors [45]. It is noted however that the high dielectric constant is beneficial for the dissociation of the lithium salts in the electrolyte, and promotes fast ionic diffusion. Therefore again a trade-off between stability and performance is observed.

The formation of passivation films on the Al surface enables Al to serve as the current collector for cathodes. However, it is difficult to use Al for anodes because of the alloying reaction between Al and Li at low potentials close to 0 V vs. Li/Li^+. An exception is $Li_4Ti_5O_{12}$ anode. Al current collectors can be used for $Li_4Ti_5O_{12}$ anodes due to their high potentials, about 1.5 V vs. Li/Li^+ [46].

3.1.2 Al foil

Al foils have been used as current collectors for cathodes since the first commercial LIB which was developed by the Asahi Kasei team led by Yoshino and produced by Sony in 1991 [47]. Apart from the excellent electrochemical stability already described, high electrical conductivity is another advantage of Al foil current collectors. Al is the fourth most conductive metal with an electrical resistivity of 2.65×10^{-8} Ωm at 20 ˚C, following Ag, Cu and Au [48]. A common question is raised regarding the effect of the insulating Al_2O_3 layer on the electrical conductivity of Al. Tian et al. measured the electrical resistivity of an Al wire using the four-probe technique [49]. The Al wire was not polished or subjected to any other treatments. Thus, an Al_2O_3 layer is expected to

form on the surface of the Al wire. The measured electrical resistance was 2.83 x 10^{-8} Ωm [49], which is very close to the value of pure Al. Similar work was done by Brandt and Neuer who reported an electrical resistance of about 2.80 x 10^{-8} Ωm [50], indicating that the Al_2O_3 layer does not affect the electrical conductivity of Al current collectors.

Low density and good mechanical properties also make Al foils stand out from other metals. Al has a low density of 2.70 g/cm^3 [48], which is favourable for increasing battery gravimetric energy density. Early Al foil current collectors have a thickness of 25 µm, which are normally manufactured by rolling thicker stock foils into thinner and thinner sheets [51]. The thickness of Al foil current collector was reduced down to 10 µm in further development to achieve high energy density. The effect of the thickness of Al foils on LIB energy density can be seen by comparing two specific LIBs, Sony VTC5A and VTC6 [16]. Both of the two Sony LIBs have an identical 18650 size, NCA cathode, graphite and silicon composite anode. The VTC6 LIB has a thinner Al foil with a thickness of 12 µm, contributing to a higher gravimetric and volumetric energy density of 246 Wh kg^{-1} and 665 Wh L^{-1}, respectively. While the counterpart (VTC5A LIB) has a 15 µm thick Al foil, resulting in a lower gravimetric and volumetric energy density of 196 Wh kg^{-1} and 552 Wh L^{-1}, respectively. However, the enhanced energy density is at cost of power density. This is in part due to the thickness of the current collectors, because the electrical conductivity and heat transfer property of Al foils decrease with thickness, but also the thickness of the electrode films. This highlights the interconnected electrode and cell engineering requirements that are required to optimise the specific properties of a cell. The VTC5A LIB has a gravimetric and volumetric power density of 2.3 kW kg^{-1} and 6.5 kW L^{-1}, respectively, higher than that of the VTC6 LIB (1.6 kW kg^{-1} and 4.2 kW L^{-1}). The Al foil current collectors with a thickness in the range of 10 – 20 µm have an estimated yield strength around 7 MPa and tensile strength around 25 MPa at room temperature [52].

The price of commercial Al foil current collectors varies significantly with different suppliers. To facilitate comparison with other materials in this study, we take the lowest online quotation from an identical supplier, Goodfellow Cambridge Ltd., Huntingdon, UK. The price of Al foil with a thickness of 20 µm and a high purity of 99% is about $ 130 /m^2. It is worth mentioning that the price of Al foil from industrial suppliers is much lower, with an estimated price of about $ 5 /m^2 in 2011 [51].

3.1.3 Al mesh

The high contact resistance is a major issue of Al mesh current collectors. Arora et al. reported the important role of the contact resistance between mesh current collectors and electrodes in battery performance by simulations [53]. The contact resistance mainly originates from the mesh current collector and ranges from 20 to 35 Ωcm^2, depending on different cell specifications [53]. Hikmet conducted an experimental study of the contact resistance between an Al mesh current collector and a $LiCoO_2$ cathode [54]. The electrical resistance of an Al mesh/$LiCoO_2$/Al mesh sandwich structure is 40 Ω, which is equivalent to the resistance of two Al mesh/$LiCoO_2$ interfaces. Given than the Al mesh current collector has a geometric surface area of 1.76 cm^2, the resistance of the Al mesh/$LiCoO_2$ interface can be converted into 35.2 Ωcm^2, which agrees with Arora's work. Hikmet also measured the contact resistance between a $LiCoO_2$ cathode and an Al film current collector which was directly deposited on the $LiCoO_2$ cathode. The deposited Al/$LiCoO_2$ interface has a resistance of 1.32 Ωcm^2, much lower than the Al mesh/$LiCoO_2$ interface. The reason for this result was not discussed by the author. We believe it is probably because of the different electrode preparation process. Although the Al mesh and deposited Al film current collectors have an identical geometric surface area, the cathode film was simply pressed on the Al mesh current collector under heat, with poor adhesion resulting, whereas the Al film current collector was deposited on the cathode film, resulting in a higher contact area and thus lower contact resistance than the Al mesh current collector.

Kanamura et al. compared the performance of $LiNi_{0.5}Mn_{1.5}O_4$ cathodes on Al mesh and Al foil current collectors [55]. Both the Al mesh and foil current collectors produced very similar initial discharge capacities of about 130 mAh g^{-1}, indicating a negligible effect of the current collector. From the 2^{nd} to 50^{th} cycle, the Al mesh current collector results in an average discharge capacity fade of 0.342 mAh g^{-1} per cycle, much higher than the Al foil current collector with an average capacity fade of 0.0819 mAh g^{-1} per cycle. The author ascribed the serious degradation in discharge capacity to the low mechanical strength of the Al mesh which cannot withstand expansion and shrinkage of the cathode during cycling.

Al meshes have also been used as current collectors for other cathodes, e.g. $LiAl_yCo_{1-y}O_2$ [56], $LiNi_{0.5}Mn_{0.5}O_2$ [57], $LiNi_{0.8}Co_{0.2}O_2$ [58], $Li_3Cr_2(PO_4)_3$ [59]. However,

the benefits and drawbacks of Al mesh current collectors were not well discussed in these studies.

3.1.4 Al foam

Al foams have been used as current collectors for LIBs due to the unique porous structures that enable high electrode mass loading. For conventional Al foil current collectors, high electrode mass loading is challenging because of the high risk of electrode delamination during cycling. An ultra-thick Al foam current collector with a thickness of 258 μm was used for $LiNi_{0.33}Mn_{0.33}Co_{0.33}O_2$ cathodes by Fritsch and his colleagues [60]. The Al foam current collector allows high electrode mass loadings of electrode active material up to 42 mg cm^{-2} and thus high capacities up to 7 mAh cm^{-2}, more than three times higher than commercial $LiNi_{0.33}Mn_{0.33}Co_{0.33}O_2$ cathodes with a thickness around 50 μm on a conventional Al foil current collector (~12 mg cm^{-2} loading and ~2 mAh cm^{-2} capacity) [61]. It should be noted that the electrode mass loading on Al foam current collectors also depends on loading techniques. The aforementioned high mass loading is achieved by slurry infiltration under vacuum. For example, another sample prepared by dip-coating on an Al foam current collector with a similar thickness, only has a mass loading of 7.8 mg cm^{-2} and low capacity of 1.24 mAh cm^{-2}. Although the two samples prepared by two different loading processes have different areal capacities, they have very similar gravimetric capacities in the range of 160 – 170 mAh g^{-1}, implying that that have a similar electrode efficiency. Therefore, Al foam current collectors can increase only absolute or areal capacity but not gravimetric capacity. Compared with Al foils, the Al foams also contribute to a much lower charge transfer resistance at the electrode/electrolyte interface, further improving the electrode performance [60].

Al current collectors with porous structures are also beneficial to increase Li-ion diffusion during cycling. Li-ion diffusion within electrodes has been regarded as the rate-determining step for LIB cycling, particularly at high current densities [62]. Du et al. prepared an Al current collector with tunnel-like pores for TiO_2 anodes [63], as shown in Fig. 2c and d. The tunnel-pores provide not only a high surface area for TiO_2 loading but also a diffusion pathway for Li-ions during cycling. The enhanced Li-ion diffusion enables fast charging/discharging. The TiO_2 anode on the porous Al current collector delivers a capacity of 95 mAh g^{-1} at a very high current rate of 100 C and remains stable after 8000 cycles.

3.1.5 Etched Al

Chemical etching is a treatment for current collectors to achieve a rough surface and better performance. Nakamura et al. investigated the effect of the surface morphology of Al current collectors on the electrochemical performance of $LiCo_{0.33}Ni_{0.33}Mn_{0.33}O_2$ cathodes [64]. Two different Al current collectors, one with and the other one without surface treatment, were employed in the study. The treatment process was probably chemical etching, judging by the surface morphology of the treated Al current collector which is covered by numerous sub-micron-sized pores, although the author only mentioned this as ‘chemical treatment'. The surface-modified Al current collector leads to almost the same capacities as the normal Al current collector at current rates smaller than 1 C, but higher capacities at higher current rates, due to improved contact resistance. Besides this, the surface-modified Al current collector also contributes to higher capacity retention after 30 cycles. Yoon et al. investigated the effect of the surface morphology of Al current collectors on the electrochemical performance of $LiCoO_2$ cathodes [65]. Two type solutions, i.e. a mixture of NaOH, Na_2CO_3, $C_6H_{11}NaO_7$ and a mixture of NaOH, $NaNO_3$, $C_6H_{11}NaO_7$, were employed to obtain different Al surface morphology after different etching time between 10 – 70 s. The etched Al foil with the roughest surface exhibits the highest discharging capacity, particularly at high current rates, up to 4 times higher than a normal Al foil current collector. The superior electrochemical performance of the surface-modified Al current collector arises from the rough surface which increases the adhesion between the current collectors and electrodes as well as reduces the charge transfer resistance of the $LiCoO_2$ cathode. The strong adhesion further avoids peeling of the electrode and maintains low contact resistance. Additionally, chemical etching slightly decreases the tensile strength but increases the surface hydrophilicity of Al current collectors [65].

Nakanishi et al. reported that the enhancement effect of etched Al current collectors on electrode performance is also affected by electrode type and active material particle size [66]. $LiCoO_2$ cathodes with large particles on a normal and etched Al foil current collector show similar performance, while $LiFePO_4$ cathodes with small particles exhibit highly increased discharge capacities when using an etched Al current collector to replace a normal Al foil current collector. However, based on these results, it is not possible to confidently solely ascribe the difference to either the effect of electrode

type or material particle size. The author also quantitatively measured the peel strength between the $LiFePO_4$ cathode and current collectors. The etched Al current collector gives rise to a 7 times stronger bond to the cathode than the normal Al current collector.

Due to enhanced adhesion and electrical conductivity of etched Al current collectors, Shin et al. proposed to use an etched Al current collector for $LiCoO_2$ cathodes in ultrafast LIBs [67]. The $LiCoO_2$ cathode on the etched Al current collector exhibits an initial capacity of 90 mAh g^{-1} at a high current rate of 10 C with 85% retention after 250 cycles. For comparison, the $LiCoO_2$ cathode on a normal Al current collector cannot work properly at such a high current rate.

3.1.6 Coated Al

Coating is an effective way to improve the conductivity of Al current collectors to achieve better electrode performance. Striebel et al. compared the performance of $LiFePO_4$ cathodes on a carbon-coated and a bare Al current collector [68]. The $LiFePO_4$ cathode on the carbon-coated Al current collector delivers a discharge capacity of 160 mAh g^{-1} at a low current rate of 0.2 C and has a 70% capacity retention at a high current rate of 5 C, while the $LiFePO_4$ cathode on the bare Al current collector delivers a discharge capacity of 140 mAh g^{-1} at 0.2 C and only has a 15% capacity retention when the current rate increases to 5 C. The $LiFePO_4$ cathode on the bare Al current collector also undergoes serious voltage drop from 3.4 to ~2.6 V vs. Li/Li^+ as the charging rate increases from 0.2 C to 5 C, indicating that the bare Al current collector brings a large contact resistance. Replacing the bare Al current collector with the carbon-coated Al current collector gives rise to a contact resistance drop from 200 to ~40 Ωcm^2 and thus a small voltage drop of 0.2 V when the charging rate increases from 0.2 C to 5 C. Furthermore, the formation of carbon coating on Al current collectors in flowing CH_4 at 600 °C can remove the native oxide on the Al surface and thus improve electrical conductivity [69].

Coating can also improve the corrosion resistance of Al current collectors. Doberdò et al. used a carbon-coated Al current collector for $LiNi_{0.33}Mn_{0.33}Co_{0.33}O_2$ cathodes with carboxymethyl cellulose (CMC) as a binder and water as a solvent [70]. Though normal Al current collectors suffer from serious corrosion when in direct contact with this $LiNi_{0.33}Mn_{0.33}Co_{0.33}O_2$ cathode slurry due to its basicity, the carbon-coated Al

current collector shows good corrosion resistance. The thickness of the carbon coating is crucial for corrosion resistance. For the Al surface coated with a 2 μm carbon layer, small corrosion pits were still visible, while no evident trace of corrosion was observed on the Al surface coated with a 5 μm carbon layer. The $LiNi_{0.33}Mn_{0.33}Co_{0.33}O_2$ cathode on the 5 μm carbon-coated Al current collector delivers a capacity of 126 mAh g^{-1} at 1 C after 50 cycles, higher than an identical cathode on a normal Al current collector (107 mAh g^{-1}).

Apart from carbon, other materials have also been coated on Al current collectors to improve electrode performance, e.g. graphene oxide [71], Mn and Al oxide composite [72], chromate [73] and graphene [74]. All of these coatings are reported to be favourable for improving either or both of the electrical conductivity and electrochemical stability of Al current collectors. Among them, the Mn and Al oxide composite and graphene coatings can also improve the adhesion between Al current collector and electrodes.

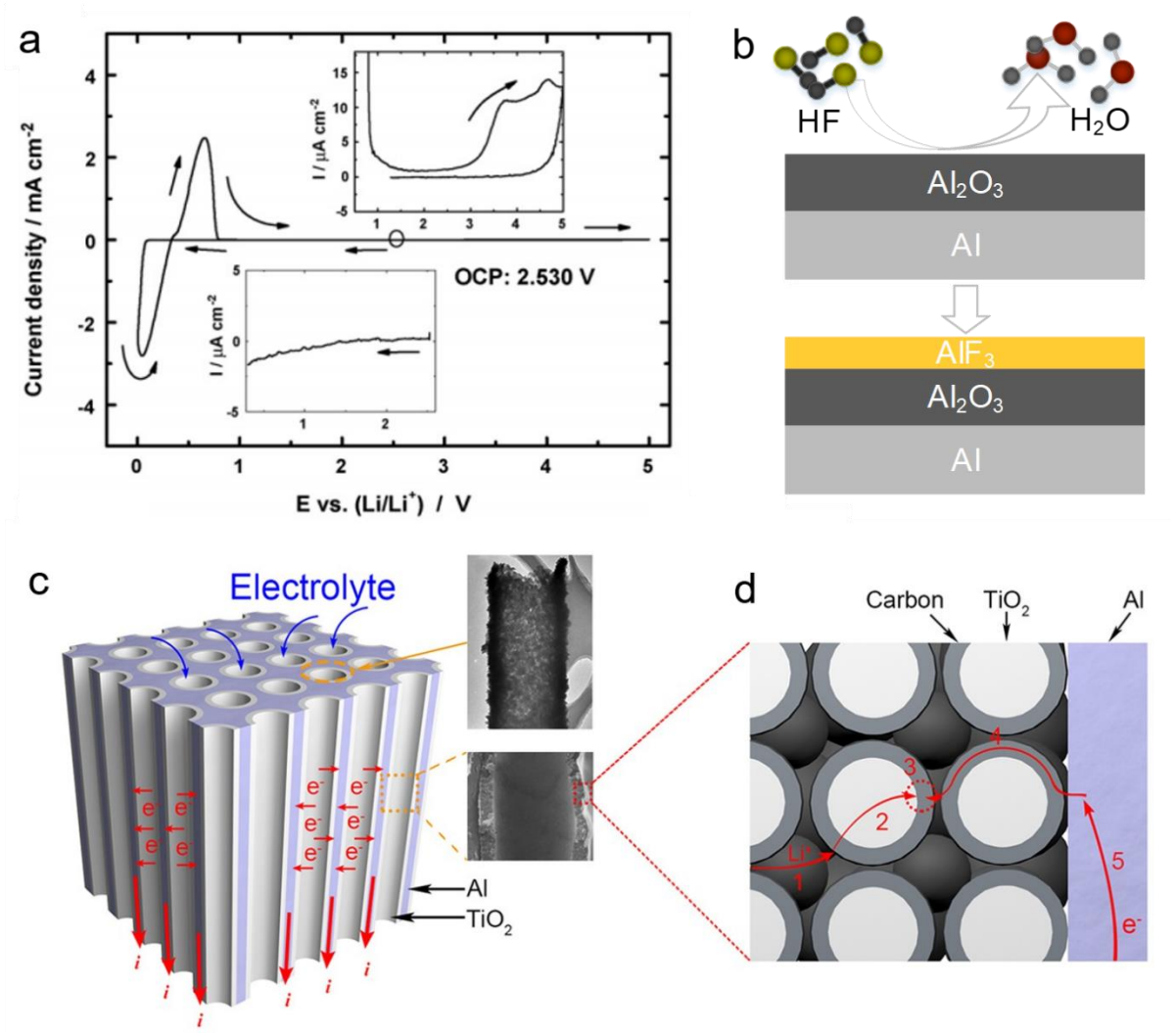

Fig. 2 a) Cyclic voltammetry of Al in 1 M $LiPF_6$ in EC:DMC (1:1 vol.%) electrolyte (Reproduced with permission [30]. Copyright 2009 Elsevier), b) schematic drawing of passivation film formed on Al surface, c) and d) tunnel-like Al foam current collector (enlarged view: 1 ion transport in the electrolyte, 2 ion transport in the electrode, 3 electrochemical reactions in the electrode, 4 electron transport in the electrode and 5 electron conduction in the current collector) [63].

Table. 1 Al current collectors

Type	Electrode	Current rate/C	Capacity/ mAh g^{-1}	Capacity retention (cycles)	Reference
Foil	LNMO	0.1	130	97% (50)	[55]
Foil	NMC111	0.1	178	91% (30)	[64]
		10	20	-	

Foil	LCO	~0.1	188	93% (50)	[65]
		~2.7	25	-	
Foil	LCO	0.2	142	-	[66]
		1	138	-	
		5	96	-	
Foil	LFP	0.2	128	-	[66]
		1	105	92% (240)	
		5	0	-	
Foil	LCO	1	120	71% (100)	[67]
		10	0	-	
Foil	LFP	0.2	140	-	[68]
		5	20	-	
Foil	NMC111	1	110	97% (50)	[70]
		10	35	-	
Foil	LMO	3	100	80% (100)	[71]
Foil	LFP	0.1	158	-	[72]
		1	145	84% (2000)	
		5	116	-	
Foil	LMO	-	130	0% (50)	[73]
Foil	LCO	0.1	150	-	[74]
		1	130	4% (50)	
		5	45	-	
Mesh	LNMO	0.1	130	87% (50)	[55]
Mesh	LNMO	0.1	174	~100% (10)	[57]
		0.5	145	90% (40)	
		2	110	-	
Foam	NMC111	0.2	166	90% (140)	[60]
		2	55	-	
Foam	TiO_2	0.3	330	-	[63]
		100	100	~100% (8000)	
Etched	NMC111	0.1	178	94% (30)	[64]
		10	25	-	
Etched	LCO	~0.1	190	96% (50)	[65]
		~2.7	125	-	

Etched	LCO	0.2	140	-	[66]
		1	138	-	
		5	104	-	
Etched	LFP	0.2	125	-	[66]
		1	114	~100% (240)	
		5	80	-	
Etched	LCO	1	135	85% (100)	[67]
		10	90	85% (250)	
Carbon-coated	LFP	0.2	160	-	[68]
		5	110	-	
Carbon-coated	NMC111	1	120 (2 µm) [a]	97% (50)	[70]
			128 (5 µm) [a]	98% (50)	
		10	51 (2 µm) [a]	-	
			60 (5 µm) [a]	-	
Graphene oxide-coated	LMO	3	100	90% (100)	[71]
Mn and Al oxide composite-coated	LFP	0.1	162	-	[72]
		1	150	95% (2000)	
		5	120	-	
Chromate-coated	LMO	-	115	87% (50)	[73]
Graphene-coated	LCO	0.1	160	-	[74]
		1	135	55% (50)	
		5	110	-	

Note: partial data were taken from published figures by approximation, '-' means data not given, as noted for other tables.

[a] denotes current collectors with specific coating thicknesses.

3.2 Cu

3.2.1 Electrochemical stability

The electrochemical behaviour of Cu in the electrolyte of $LiPF_6$ in EC:DMC (1:1) is shown in Fig. 3a. An open circuit potential at 3.326 V vs Li/Li^+ is initially observed, the first cathodic peak can be seen at about 3.1 V vs Li/Li^{+1}, which is suggested to correspond to the decomposition of $LiPF_6$ to HF [75]. A large cathodic peak is observed between 1.5 – 3 V vs Li/Li^+, which corresponds to the reduction process of the air-formed Cu oxide film to metal, the electrolytic salt formation of Li_2O, the reduction of

the solvent and the formation of the solid electrolytic interphase (SEI) layer on the Cu surface [30, 44]. A small cathodic peak and anodic peak at about 0.6 V and 0.7 V vs Li/Li^+ represent underpotential deposition of Li on the Cu surface and subsequent dissolution of the deposited Li in the electrolyte, respectively [30, 44]. As Cu is polarized in the anodic direction, no other peak appears until approaching a high potential of 3.5 V vs Li/Li^+. The anodic peak at about 3.7 V vs Li/Li^+ has been identified as the dissolution of Cu into the electrolyte [30, 44]. Similar dissolution behaviours of Cu in other electrolytes of $LiPF_6$ in EC:DEC (1:1 vol.%), $LiClO_4$ in EC:DEC(1:1 vol.%) and $LiClO_4$ in PC at high potentials were also reported by Iwakura et al. [76] and Kawakita et al. [77]. The dissolution of Cu can cause numerous pits with a characteristic shape which looks like a hole with the square aperture area advanced toward the inside of the substrate, as shown in Fig. 3b. Therefore, the dissolution of Cu is also named 'pitting corrosion' in many studies.

A small amount of water and HF can boost the dissolution of Cu [78]. The mechanism was proposed by Dai and his colleagues [79]. As shown in Eqs. 4 – 5, Cu is first oxidized by water with the formation of Cu oxide. The Cu oxide further reacts with HF either generated from the decomposition of $LiPF_6$ or introduced externally, producing CuF_2. Both CuO and CuF_2 have been proven to exist on the Cu surface after immersion in the electrolyte of $LiPF_6$ in EC:DMC (1:1 vol.%) [30, 44]. Nevertheless, they do not form a substantial passivation film on the Cu surface. The dissolution of Cu can also be affected by electrolytes. It was found that Cu is more readily dissolved in the solvent of PC:EC:DMC (1:1:3 vol.%) than EC:DMC:DEC (2:2:1 vol.%) and EC:DMC:MEC (1:1:1 vol.%) at the same potentials [78]. However, the reason is still not clear.

$$Cu + xH_2O \rightarrow CuO_x + 2xH^+2xe^- \quad \text{Eq. 4}$$

$$CuO_x + 2xHF \rightarrow CuF_2 + xH_2O \quad \text{Eq. 5}$$

Though the dissolution of Cu at high potentials hinders Cu serving as the current collector for cathodes, the stable electrochemical behaviour of Cu at potentials below 3 V vs Li/Li^+ as well as no alloying reactions with Li make Cu a good choice for current collectors at anodes because most anodes have low potentials. However, over-discharging may raise the potential of anodes, causing severe Cu dissolution. The dissolved Cu ions will redeposit as Cu metal at anodes to form dendrites and pierce

the separator, resulting in capacity fading and short-circuit of LIBs [80]. Therefore, over-discharging should be avoided when using Cu current collectors for anodes.

3.2.2 Cu foil

Almost all commercial LIBs use Cu foils as current collectors for anodes since the first LIB produced by Sony [47]. The initial Cu foils were manufactured by rolling and therefore low levels of oil were present upon the surface, this caused adhesion issues, and therefore needed to be removed before use [81]. More recently Cu foils are manufactured by electrodeposition methods [82]. Apart from the good electrochemical stability aforementioned, Cu is the second most conductive metal with a resistivity of 1.68×10^{-8} Ωm at 20 ˚C [48], which is another advantage of using Cu current collectors. However, Cu is much heavier than Al with a density of 8.96 g/cm^3 [48]. The high density of Cu results in Cu foil current collectors occupying more than 10% of the total weight of LIBs, about twice of the Al foil current collector for cathodes [13].

Similar to Al foil current collectors, Cu foil current collectors tend to be thinner and thinner for the pursuit of high energy density [16]. Two specific LIBs, Samsung 30Q and Sony VTC5A, have an identical battery size, cathode and anode, as well as very similar battery design. The Samsung 30Q LIB has a 10 µm Cu foil current collector, thinner than the Sony VTC5A (14 µm). The Samsung 30Q LIB has a gravimetric and volumetric energy density of 245 Wh kg^{-1} and 657 Wh L^{-1}, respectively, higher than the Sony VTC5A (196 Wh kg^{-1} and 552 Wh L^{-1}). However, the thinner Cu foil current collector and coated electrodes of the Samsung 30Q LIB results in a lower gravimetric and volumetric power density of 1.2 kW kg^{-1} and 3.2 kW L^{-1}, respectively, compared with the Sony VTC5A having a gravimetric and volumetric power density of 2.3 kW kg^{-1} and 6.5 kW L^{-1}. This highlights, similar to the aluminium current collector and cathode, that the combination of electrode and cell design is important when optimising the performance properties of a cell.

Special concern has been expressed over the mechanical strength of Cu foil current collectors because Cu foils may suffer from environmentally assisted cracking and structure degradation during repeated battery cycling under bending stress [34]. Recent work also reported that Cu foil current collectors for Sn-based anodes underwent structural degradation during cycling [83]. The mechanical properties of commercial Cu foil current collectors were systematically investigated by Zhu and his

colleagues [84]. The elastic modulus, tensile, fracture and yield strengths of Cu foils with a thickness of 8 – 35 μm are in the ranges of 45 – 75 GPa, 300 – 350 MPa, 260 – 360 MPa and 40 – 180 MPa, respectively, which is higher than that of Al foils.

At the time of writing, the cost of Cu foils with a thickness of 20 μm and a purity of 99.9% is about $ 640 /m^2, from the online quote of Goodfellow, much higher than that of Al foils.

3.2.3 Cu mesh

Li et al. used Cu meshes as current collectors for Li metal anodes [85]. To connect the Cu mesh current collector and Li metal anode, a circle-shaped copper mesh with a pore diameter in the range of 60 – 170 μm was aligned with a Li metal foil and pressed with a punching machine until the Cu mesh was fully embedded in the Li metal. The Li metal anode on the Cu mesh current collector exhibits much better cycling performance than that on a conventional Cu foil current collector, with a high coulombic efficiency of 93.8% after 100 cycles against a low coulombic efficiency of 30.9% after 70 cycles at a current rate around 0.5 C, respectively. When used in a Li/ $Li_4Ti_5O_{12}$ cell, the Li metal anode on the Cu mesh current collector results in a higher cell capacity than a bare Li metal anode, particularly at high current rates. The enhanced performance of the Cu mesh current collector can be attributed to four aspects. 1) the presence of holes on the Cu mesh enhances the charge transfer kinetics and reduces the electrode/electrolyte interfacial resistance. Li anode on the Cu mesh current collector has a low electrode/electrolyte interface resistance of 27 Ωcm^2 after 10 cycles, while a bare Li anode shows a high interface resistance of 62 Ωcm^2. 2) The Cu mesh current collector can accommodate the volume change of Li anode to some extent during battery cycling. This unique function also makes Cu mesh a good current collector for Si-based anodes that suffer from severe volume change [86, 87]. 3) The high surface area of Cu meshes lowers the areal current density, leading to uniform charge distribution and thus smoothening the Li deposition and preventing Li dendrite formation [88]. 4) The thickness of the anode remains almost unchanged during cycling, providing good mechanical stability of the anode and integrity of cells.

3.2.4 Cu foam

Cu foams can bring many benefits when used as current collectors, particularly for Li metal anodes that have high theoretical capacity but suffer from severe volume change and Li dendrite formation. The porous structure of Cu foams can greatly accommodate the volume expansion/contraction of Li metal anodes during cycling. Besides, Cu foams provide much higher surface areas than Cu foils, which lowers the local current density and in turn prevents Li dendrite formation. Therefore, Cu foams are ideal current collectors for Li metal anodes from this point of view. A typical example of using Cu foams as current collectors to improve Li anode performance is reported by Yun and his colleagues [89]. They fabricated Cu foams with a pore size in the range of 0.2 – 2 μm by chemical dealloying of CuZn. The as-fabricated Cu foam current collector results in a coulombic efficiency over 95% at 1 C after 150 cycles, much better than a conventional Cu foil current collector with a coulombic efficiency of 80% under the same measurement conditions. Similar conclusions have also been drawn from other studies [90, 91].

Cu foam current collectors with pores neither too big nor small are appropriate for improving Li metal anode performance. Small pores, e.g. nano-sized pores, can prevent Li dendrite formation due to high surface area but suffer from the volume change of Li metal anodes. By contrast, large pores, e.g. micron-sized pores, can accommodate the volume change but only provide limited surface area. Liu et al. developed a hierarchical Cu foam current collector with both micron- and nano-sized pores for Li metal anodes, providing a good solution for this problem. The micron- and nano-sized pores are formed by physical dealloying and immersion in a NaOH and $(NH_4)_2S_2O_8$ mixed solution, respectively. The micron-sized pores effectively accommodate the volume change of the Li metal anodes during cycling and the nano-sized pores increase total surface area and prevent Li dendrite formation [92]. The surface area of a hierarchical Cu foam containing both micron- and nano-sized pores can be up to 60 times higher than that of a Cu foam only containing micron-sized pores [93]. The as-produced hierarchical Cu foam results in a high coulombic efficiency more than 98% at 1 mA cm^{-2} after 200 cycles, better than a Cu foam only with micron-sized pores (90% after 200 cycles) and a conventional Cu foil (23% after 150 cycles).

The pore geometry is also key for Cu foam current collectors. Wang et al. developed a Cu foam current collector with vertically aligned microchannels for Li metal anodes

[94]. The vertically aligned microchannels exhibit a tip effect, leading to preferential nucleation of Li inside the mouth of channels and preferential deposition on the microchannel walls and thus effectively restraining growth of Li dendrites. The tip effect essentially means the surface with a high curvature has high surface potential due to the distortion of the electrical field, which makes Li dendrites form more readily [95]. The geometry of the microchannels, i.e. radius, depth and spacing, can also affect battery performance. With optimised microchannel geometry, the Li anode on the vertically aligned microchannels current collector exhibits a high stable coulombic efficiency around 98.5% at 1 mA cm^{-2} within 200 cycles, much better than conventional Cu foil current collectors with a coulombic efficiency dropping from 98% in the 1st cycle to 50% after 80 cycles. Wang et al. fabricated Cu foam current collectors through a NaCl-assisted powder sintering process [96]. The produced Cu foam has interconnected micron-sized pores with a smooth inner surface, which provides high surface area and facilitates Li-ions diffusion, resulting in uniform Li deposition and effectively suppressing Li dendrite formation. The as-fabricated interconnected Cu foam contributes to a coulombic efficiency higher than 90% at 1 mA cm^{-2} after 400 cycles. For comparison, the commercial Cu foams manufactured by electrodeposition only results in a coulombic efficiency of 50% at 1 mA cm^{-2} after 300 cycles.

Cu foam current collectors can also bring many benefits to other anodes apart from Li metal anodes. For example, Cu foams with a porosity of 97% enable fabrication of thick graphite anodes with a thickness of up to 1.2 mm which is 10 times greater than conventional Cu foils [97]. The thick graphite anode greatly improves the energy density of LIBs but sacrifices the observed gravimetric capacity due to increased internal resistance. The gravimetric capacity of the graphite anode decreases from 375 to 275 mAh g^{-1} as the electrode thickness increases from 0.3 to 1.2 mm. The author solely ascribed the reduced gravimetric capacity to increased electronic resistance, which is evidenced by the result that the voltage hysteresis between the charge and discharge is smaller for the thinner electrode. We believe not only the electronic resistance but also Li-ion diffusion reduces the gravimetric capacity of thick electrodes. Because the thick electrode is difficult for Li-ions to diffuse through and can cause Li-ion depletion in the electrolyte phase [98]. Additionally, Cu foams can effectively accommodate the volume change of Si and Sn anodes during battery cycling [99, 100]. When used as current collectors for Sn anodes, the phase

transformation of Sn into Cu_6Sn_5 takes place on the electrode/current collector interface. The newly-formed phase Cu_6Sn_5 enhances the bonding force between Sn anodes and Cu foam current collectors, further restraining the volume changes of active materials during cycling [100].

3.2.5 Etched Cu

Cu current collectors with a rough surface are favourable to improving electrode performance [101, 102]. Nguyen et al. used an etched Cu current collector for amorphous Si anodes [103]. The rough surface of the etched Cu provides a high contact area and thus strong adhesion to the Si anode as well as good electrical conductivity. Meanwhile, the etched holes existing on the surface are filled up with Si, indicating a higher mass loading than Cu foils. With the help of a siloxane-stabilized electrode/electrolyte interface, the Si anode on the etched Cu current collector exhibits a discharge capacity up to 4255 mAh g^{-1}, versus 2428 mAh g^{-1} for the Si anode on an unetched Cu current collector. The discharge capacities of the Si anodes on the etched and unetched Cu current collectors remain at 80% and 53% after 200 cycles, respectively. A similar study was conducted by Reyter and his colleagues who used etched Cu current collectors for Si powder anodes [104]. The etched Cu contributes to a high capacity up to 2410 mAh g^{-1} at 600 mA g^{-1} after 25 cycles versus 1630 mAh g^{-1} for an unetched Cu current collector. They also quantitatively compared the adhesion strength between the Cu current collectors and Si anodes through a scratch test. The minimum load in grams required to scrape through the Si anode to the etched and unetched Cu current collectors are 110 and 40 g, respectively, proving that the eteched surface provides a stronger adhesion to the Si anode.

Selective etching on Cu current collectors can effectively alleviate the volume change of Si anodes during cycling. Cho et al. selectively etched Cu foils with discontinuous lines at regular spacings and subsequently deposited Si on the etched Cu current collectors to obtain discontinuous Si anodes [105]. The discontinuous Si anode exhibits better cycle stability than continuous Si anodes, i.e. Si deposited on a conventional Cu foil current collector. The enhanced cycle stability is attributed to the discontinuous lines that accommodate the stress generated by the volume change of Si anodes. Three different spacings between the discontinuous lines of 400, 800, 1700 μm were made to investigate the effect of spacing, with the smallest spacing of 400 μm resulting in the best performance. Cho et al. further developed trench-structured

Cu current collectors for Si anodes following a similar selective etching and deposition process [106]. Si film was deposited on either the whole surface of the etched Cu current collector or only the bottom of the trenches, termed wholly covered Si film anode or selectively covered Si film anode, respectively, as shown in Fig. 3c-e. The wholly covered Si anode exhibits an 18.5% increase in initial capacity compared to the continuous Si film anodes. The selectively covered Si film anode shows even better performance than the wholly covered one. The geometry of the etched trenches has modest effects on the Si anode performance, with a trench width of 45 μm and trench height of 14 μm resulting in the highest columbic efficiency and best cycle performance.

3.2.6 Coated Cu

Cu current collectors with various material coatings can provide many benefits. Kang et al. coated conventional Cu foils with a rough layer of carbon via an electric discharge method and used the carbon-coated Cu foils as current collectors for graphite anodes [107]. The carbon-coated Cu current collector shows reduced electrical and charge transfer resistance, resulting in higher capacity and better rate capability than conventional Cu foil current collectors. Wu et al. prepared carbon-coated Cu current collectors via chemical vapour deposition at 600 ˚C and subsequently used the as-prepared current collectors for $Li_4Ti_5O_{12}$ anodes [69]. In addition to improved electrical and charge transfer properties, the carbon-coated Cu current collector prepared at high temperature shows greater surface hydrophobicity than conventional Cu foils, which improves the surface adhesion to the $Li_4Ti_5O_{12}$ anode. More importantly, $Li_4Ti_5O_{12}$ anode is known to have a high voltage plateau at about 1.55 V vs Li/Li^+ during cycling, which is challenging for Cu current collectors due to low corrosion resistance at high potentials. The carbon coating is expected to provide a protective film for Cu against corrosion, leading to improved cycle stability. Similar benefits can also be found from graphene-coated Cu current collectors [108]. The graphene coating on Cu current collectors brings up to 32% increase in the capacity of $Li_4Ti_5O_{12}$ anodes due to enhanced electrical conductivity, charge transfer kinetics, adhesion to anodes and electrochemical stability.

Coating is an effective way to make the surface of current collectors lithiophilic. Zhang et al. constructed a Cu current collector coated with vertically aligned CuO nanosheets via NH_4OH etching for Li metal anodes [109]. The Li metal anode on the CuO-coated Cu current collector provides a high coulombic efficiency of 94% at a current density

of 1 mA cm^{-2} for 180 cycles, in contrast to a conventional Cu current collector with a coulombic efficiency less than 20% after 150 cycles. A prolonged lifespan of 700 h at 0.5 mA cm^{-2} is also easily achieved. The enhanced performance arises from the lithiophilic CuO coating which can reduce the nucleation overpotential and guide uniform Li nucleation and deposition [110]. Ag is another lithiophilic material which has been used to coat Cu current collectors [111]. The Li metal anode on the Ag-coated Cu foil exhibits a stable coulombic efficiency of 98% for 50 cycles at a current density of 1 mA cm^{-2} versus 95% for 20 cycles for uncoated Cu foils. The Ag-coated Cu current collector results in an improved lifespan of up to 360 h at 1 mA cm^{-2}, more than twice of the uncoated Cu foil current collector. Other materials, such as Ni and ZnO, can also be coated to make the Cu surface lithiophilic [112, 113]. It is worth mentioning that the Li metal anodes also benefit from the nanostructures of CuO and Ag which can facilitate fast Li-ion diffusion and reduce the local current density.

Artificial SEI can also be directly coated on Cu current collectors to improve electrode performance. Luo et al. coated Cu current collectors with a thin layer of high-polarity β-PVDF for Li metal anodes [114]. The β-PVDF has all trans conformation with F and H atoms located on the opposite sides of the polymer backbone, serving as an artificial SEI to facilitate uniform Li deposition by the strong interactions between its polar functional groups and Li-ions. The β-PVDF-coated Cu current collector enables uniform Li deposition/stripping at high current densities up to 5 mA cm^{-2}, Li-plating capacity loadings of up to 4 mAh cm^{-2}, and excellent cycling stability over hundreds of cycles.

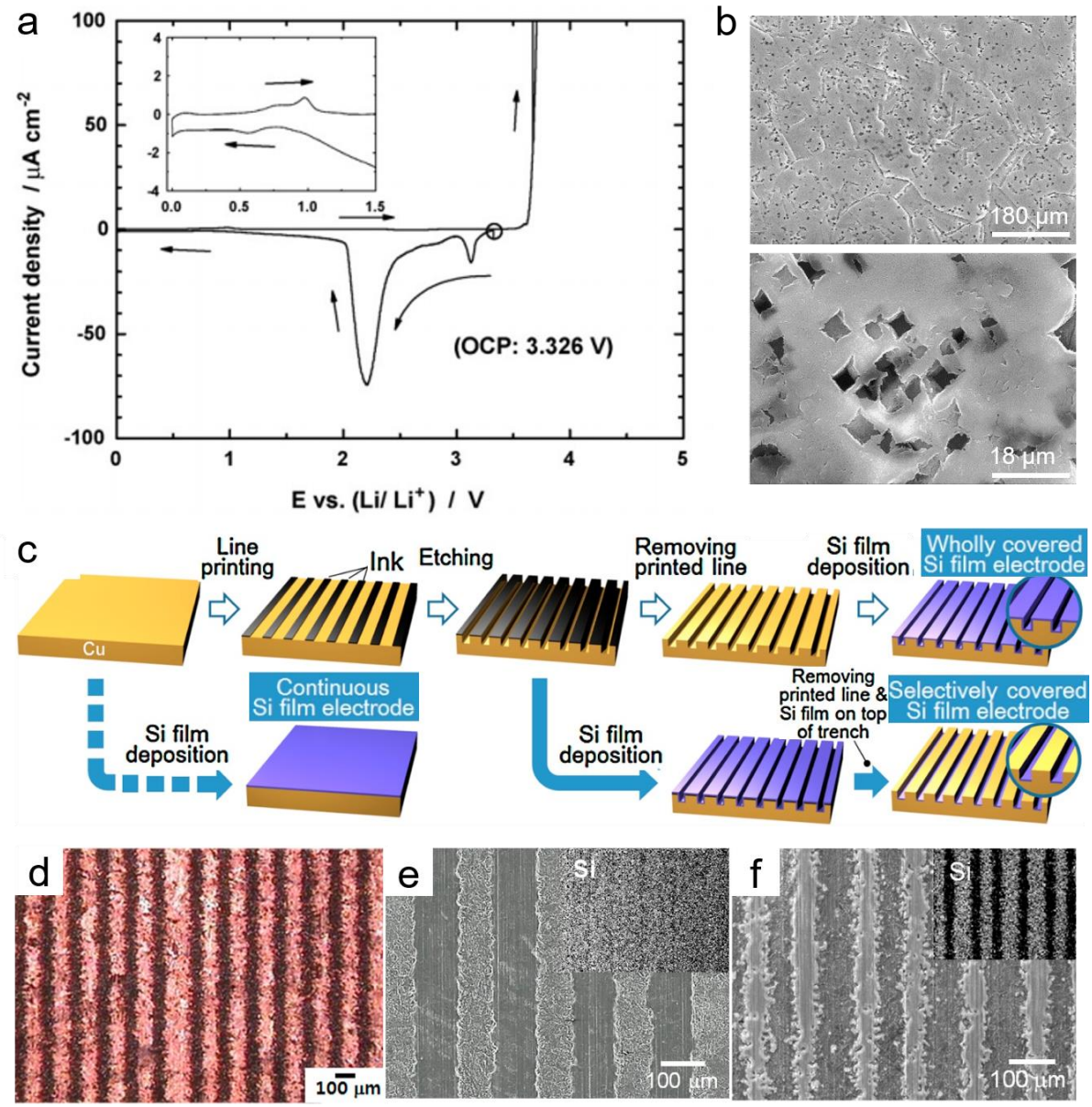

Fig. 3 Cyclic voltammetry of Cu in 1 M $LiPF_6$ in EC:DMC (1:1 vol.%) electrolyte (Reproduced with permission [30]. Copyright 2009 Elsevier), b) pitting corrosion on Cu surface (Reproduced with permission [77]. Copyright 2001 Elsevier), c) fabrication process for continuous, wholly covered and selectively covered Si film anodes, d) etched Cu current collector, e) wholly covered Si film anode, f) selectively covered Si film anode, c-f from (Reproduced with permission [106]. Copyright 2017 Elsevier).

Table. 2 Cu current collectors

Type	Electrode(s)	Current rate/C	Capacity/ mAh g^{-1}	Capacity retention (cycles)	Reference

Foil	LTO	1	155	-	[69]
		20	65	-	
Foil	Li/LFP	0.5	150	58% (300)	[89]
Foil	Li/NMC11	50 [a]	150	60% (300)	[90]
Foil	Li/LFP	2	110	33% (200)	[91]
Foil	Li/LFP	0.5	150	~100% (50)	[92]
Foil	Li/LFP	0.5	149	80% (100)	[94]
		5	15	-	
Foil	Si	-	800	85% (40)	[99]
Foil	Sn	100 [a]	300	75% (20)	[100]
Foil	Si	0.035 [a]	2428	53% (200)	[103]
Foil	Si	600 [a]	3250	50% (25)	[104]
Foil	Si	0.5	2021	10% (35)	[106]
Foil	C/LFP	1	955	96% (400)	[107]
		4	888	-	
Foil	LTO	0.1	151	-	[108]
		2	126	85% (200)	
		10	84	-	
Foil	Li/LFP	0.1	160	-	[109]
		0.5	150	57% (300)	
		5	120	-	
Foil	Li/LFP	0.2	115	-	[111]
		1	55	92% (200)	
		2	30	-	
Mesh	Li/ LTO	0.2	145	-	[85]
		4	85	80% (500)	
		10	60	-	
Foam	Li/LFP	0.5	150	90% (300)	[89]
Foam	Li/NMC111	50 [a]	150	90% (300)	[90]
Foam	Li/LFP	2	120	75% (200)	[91]
Foam	Li/LFP	0.5	151	~100% (50)	[92]
Foam	Li/LFP	0.5	149	90% (100)	[94]
		5	45	-	
Foam	Li/LFP	1	158	90% (200)	[96]
		10	124	-	

Foam	Graphite	0.2	285 (1.2 mm) [b]	-	[97]
			335 (0.6 mm) [b]	-	
			370 (0.3 mm) [b]	-	
Foam	Si	-	800	~100% (60)	[99]
Foam	Sn	100 [a]	850	59% (50)	[100]
Etched	Si	0.035 [a]	4255	80% (200)	[103]
Etched	Si	600 [a]	3250	74% (25)	[104]
Etched (wholely)	Si	0.5	2267	48% (100)	[106]
Etched (selectively)	Si	0.5	2758	71% (100)	[106]
Carbon-coated	LTO	1	160	-	[69]
		20	80	-	
Carbon-coated	C/LFP	1	996	97%(400)	[107]
		4	946	-	
Graphene-coated	LTO	0.1	155	-	[108]
		2	132	97% (200)	
		10	107	-	
CuO-coated	Li/LFP	0.1	160	-	[109]
		0.5	150	81% (300)	
		5	125	-	
Ag-coated	Li/LFP	0.2	125	-	[111]
		1	72	98% (200)	
		2	50	-	
Ni-coated	Li/LCO	0.2	120	-	[112]
		5	90	96% (250)	
		10	30	-	
ZnO-coated	Li/LCO	1	153	-	[113]
		10	99	84% (1000)	
		30	78	-	
β-PVDF-coated	Li/LFP	0.3	150	96% (40) 47% (100)	[114]

Note: When current collectors are tested in full cells, the 2nd column is expressed as anode/cathode, as noted for other tables.

[a] denotes a different unit of mA g^{-1} for current rate.

[b] denotes specific electrode thicknesses.

3.3 Ni

3.3.1 Electrochemical stability

Zhuang et al. performed a cyclic voltammetry study of Ni in 1.2 M $LiPF_6$ in EC:EMC (3:7 vol.%) electrolyte, in a potential range from 0.5 – 2.9 V vs. Li/Li^+, as shown in Fig. 4a [115]. A large cathodic peak can be seen at 1.85 V vs. Li/Li^+ in the first cycle, which is probably due to the reduction of Ni oxide to Ni and the formation of the SEI on the Ni surface. A further shift of the potential in the cathodic direction probably results in underpotential deposition of Li on the Ni surface. No alloying reaction was observed as the potential moved close to 0 V vs. Li/Li^+ [116]. The peaks in the anodic direction were not well explained by the authors, which may arise from the dissolution of deposited Li, oxidation of Ni and decomposition of the SEI. After the first cycle, the overall current density remains below 5 μA cm^{-2}, indicating good electrochemical stability in this potential range. Therefore, it is possible to use Ni as current collectors for anodes.

The electrochemical behaviour of Ni in the electrolytes of 1 M $LiClO_4$ in ethylene carbonate (EC):diglyme (DG) (1:1 vol.%) and 1 M $LiPF_6$ in EC:DG (1:1 vol.%) in a high potential range of 3 – 5.5 V vs Li/Li^+ was investigated by Geoffroy et al. [117]. It was reported that Ni was stable in the electrolytes up to 4.5 V vs Li/Li^+. However, different conclusions were drawn by other studies. Liu et al. reported that Ni corroded at a potential of 3.6 V vs Li/Li^+ in $LiPF_6$ in EC/DMC/DEC (1:1:1 vol.%) electrolyte [118]. Veith and Dudney proposed that Ni promoted the electrochemical degradation of electrolytes containing $LiPF_6$ at potentials higher than 3.5 V vs Li/Li^+ [119]. Overall, the electrochemical behaviour of Ni current collectors has not been well studied, particularly at high potentials, which hinders its application as current collectors for cathodes.

3.3.2 Ni current collector

Ni foils have been used as current collectors for many anodes, e.g. Si [120, 121], SnO_2 [122], graphene [123], Sn/graphene composite [124], Co_3O_4 [125], NiO [126] and Ni_3S_2 [127], indicating a broad applicability. Compared with Cu foils, Ni foils have a very similar density of 8.90 g/cm^3 and a higher resistivity of 6.93 x 10^{-8} Ωm at 20 ˚C [56]. The tensile strength of 20 μm thick Ni foils made by electrodeposition is 730 MPa [128], which is higher than that of Cu foils. The cost of Ni foils with a thickness of 20 μm and a purity of 99.9% is about $ 795 $/m^2$, from the online quote of Goodfellow.

Ni current collectors have a unique advantage when used as current collectors for Ni oxide and sulfide anodes, Ni can serve as not only the current collector but also a source of the metal precursor. Varghese et al. fabricated vertically aligned NiO nanowalls directly on a Ni foil using a plasma-assisted oxidation method [126]. The as-fabricated NiO anode exhibits a reversible capacity of about 638 mAh g^{-1} at a current rate of 1.25 C after 85 cycles, which is close to the theoretical capacity of 718 mAh g^{-1} [129]. Similarly, Lai et al. grew Ni_3S_2 nanowires directly on Ni substrates (Fig. 4b) [127]. The Ni_3S_2 anode delivers a reversible capacity of about 340 mAh g^{-1} at 0.1 C after 100 cycles, which is about 65% of the theoretical capacity [130]. The direct fabrication of Ni oxide and sulfide anodes on the Ni foils provides a good bonding between anodes and current collectors and eliminates the need of using binders, resulting in improved electrode performance.

Ni mesh [131, 132], foam [133-145] and etched Ni [146-148], have also been used as current collectors for LIBs. Table 3 summarizes various Ni current collectors developed for LIBs during the past two decades. Generally, the benefits from the mesh and foam structures as well as surface modification for Ni current collectors are quite similar to that for Al and Cu current collectors.

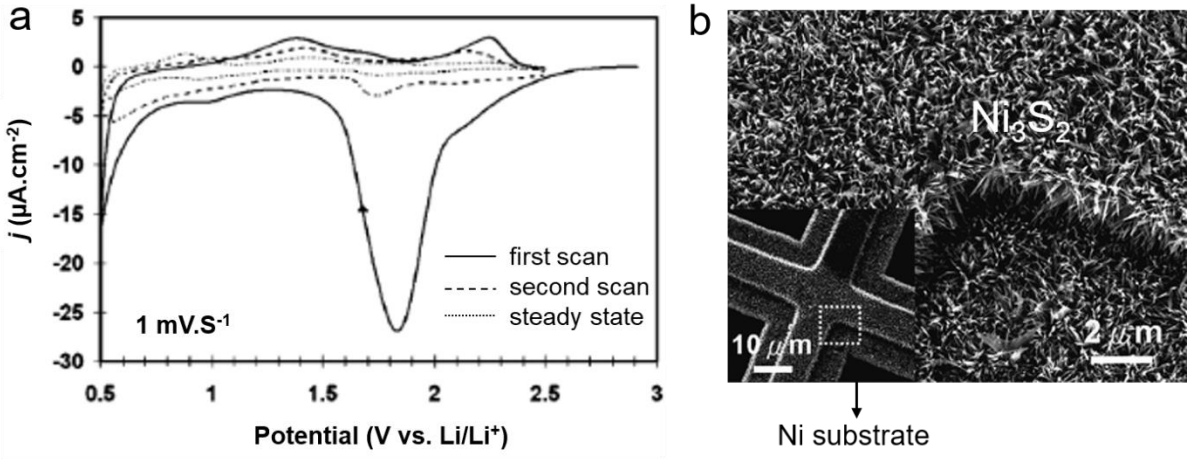

Fig. 4 a) Cyclic voltammogram of Ni electrode in 1.2 M $LiPF_6$ in EC:EMC (3:7 vol.%) electrolyte (Reproduced with permission [115]. Copyright 2005 Elsevier), b) SEM image of Ni_3S_2 nanoarrays grown on a Ni substrate (Reproduced with permission [127]. Copyright 2009 Royal Society of Chemistry).

Table. 3 Ni current collectors

Type	Electrode	Current rate/C	Capacity/ mAh g^{-1}	Capacity retention (cycles)	Reference
Foil	Si	2	1700	59% (1250)	[120]
Foil	Si	1	3700	~100% (200)	[121]
		2	3500	~100% (200)	
Foil	SnO_2	0.1	1121	58% (100)	[122]
		5	350	-	
Foil	Graphene	0.17	400	-	[123]
		2.67	280	-	
Foil	Sn and graphene composite	1	466	~100% (4000)	[124]
		2	300	-	
Foil	Co_3O_4	1	1000	105% (20)	[125]
Foil	NiO	0.62	800	92% (40)	[126]
		1.25	638	97% (85)	
		1.86	500	~100% (50)	
Foil	Ni_3S_2	0.1	400	80% (100)	[127]
Foil	Si (100 nm) [a]	1	2600	77% (400)	[147]
	Si (200 nm) [a]	1	1500	13% (500)	
Mesh	SnSb	60 [b]	500	60% (50)	[131]
Mesh	NiO	100 [b]	900	94% (20)	[132]
		10000 [b]	700	86% (20)	
Foam	C and Si composite	0.07	700	50% (95)	[133]
Foam	NiO	0.4	1.4 [c]	~100% (140)	[134]
Foam	NiO	0.5	844	85% (200)	[135]
		20	170	-	
Foam	NiO	156 [b]	701	92% (65)	[136]
		1310 [b]	200	-	
Foam	NiO	1000 [b]	706	95% (70)	[137]
		2000 [b]	548	80% (70)	
Foam	NiS	0.15	591	93% (100)	[138]
		5	394	-	
Foam	Ni_3S_2	35 [b]	451	92% (80)	[139]
Foam	Si	0.2	2500	80% (100)	[140]
		4	803	-	

Foam	Si	0.025	2500	-	[141]
		0.5	1300	88% (100)	
		4	740	-	
Foam	$ZnCo_2O_4$	500 [b]	1400	80% (50)	[142]
		1000 [b]	1300	72% (50)	
		2000 [b]	1100	49% (50)	
Foam	$ZnCo_2O_4$	200 [b]	1986	-	[143]
		400 [b]	1900	130% (300)	
		5000 [b]	811	-	
Foam	$ZnCo_2O_4$	100 [b]	1150	96% (60)	[144]
		416 [b]	1150	78%(50)	
Foam	Mn-doped Zn_2GeO_4	100 [b]	1500	87% (100)	[145]
		2000 [b]	500	-	
Etched	Si	1	2400	75% (200)	[146]
Etched	Si	-	2650	66% (200)	[147]
Etched	Si (0.67 µm) [a]	1	2250	84% (200)	[148]
	Si (1.1 µm) [a]	1	2650	66% (200)	
	Si (1.8 µm) [a]	1	2800	39% (200)	
	Si (3.6 µm) [a]	1	1400	36% (60)	

[a] denotes specific electrode thicknesses.

[b] denotes a different unit of mA g^{-1} for current rate.

[c] denotes a different unit of mAh cm^{-2} for capacity.

3.4 Ti

3.4.1 Electrochemical stability

The electrochemical behaviour of Ti in 1 M $LiPF_6$ in EC:DMC (1:1 vol.%) electrolyte was systematically investigated by Myung et al. (Fig. 5a) [30]. In the cathodic direction, a small cathodic peak at 1.7 – 2.6 V vs Li/Li^+ originates from the formation of the SEI layer on the Ti surface. Further polarization results in the reduction of the air-formed Ti oxide to Ti metal and underpotential deposition of Li on the Ti surface below 1.5V vs. Li/Li^+. Ti does not induce alloy formation with Li at low potentials close to 0. In the anodic direction, an anodic peak at about 1.6 V vs Li/Li^+ results from the oxidation of the deposited Li and Ti metal. Similar to Al, further anodic polarization leads to the formation of a passivation film which contains an outer layer of TiF_4 and an inner layer of TiO_2 on the surface of the Ti metal (Fig. 5b), providing a relatively good corrosion

resistance at high potentials [76]. However, the passivation layer on the Ti surface may not be as stable as that on the Al surface at high potentials, resulting in an inferior performance when used as current collectors for cathodes [55]. Taken together, Ti is stable in a wide potential range from 0 – 5 V vs Li/Li^+ and can serve as current collectors for both cathodes and anodes.

3.4.2 Ti current collector

Ti has a low density of 4.51 g/cm^3 [56], lower than Cu and Ni but slightly higher than Al. Ti foils with a thickness of 20 – 30 μm have a yield and tensile strength of 250 and 360 MPa [149], respectively, which is higher than Cu and Al. Adversely, Ti has a high electrical resistivity of 3.9 x 10^{-7} Ωm at 20 ˚C [56], one order of magnitude higher than the aforementioned metals. The cost of Ti foil with a thickness of 20 μm and a purity of 99.9% is as high as about $ 3100 /m^2, from the online quote of Goodfellow.

Ti foils have been used as current collectors for various electrodes, including CoO [150], Co_3O_4 [151-154], SnO_2 [155, 156], Fe_2O_3 [157], TiO_2 [158, 159] and $Li_4Ti_5O_{12}$ [160, 161], as shown in Table 4. Ti can serve as a source of metal precursor when used as current collectors for TiO_2 and $Li_4Ti_5O_{12}$ anodes. Besides, CoO, Co_3O_4, TiO_2 and $Li_4Ti_5O_{12}$ can directly grow on Ti surface without auxiliary binders and carbon black, which is favourable to improving electrode capacity and cycle stability. A typical example was done by Chen and his colleagues who fabricated $Li_4Ti_5O_{12}$ anodes on a Ti foil current collector via a hydrothermal process without any additives [160]. The as-fabricated $Li_4Ti_5O_{12}$ (Fig. 5c) exhibits a capacity of 124 mAh g^{-1} at 50 C after 3000 cycles. Similar capacities of 153 and 115 mAh g^{-1} at 2 C and 20 C after 5000 cycles, respectively, were also reported for binder-free $Li_4Ti_5O_{12}$ anodes by Wang et al. [161]. For comparison, a conventional $Li_4Ti_5O_{12}$ anode with 20% carbon black and 10% PVDF binder only delivers a capacity of 25 mAh g^{-1} at 2 C after 2000 cycles (Fig. 5d).

Table 4 also summarizes Ti mesh and foam current collectors reported in the literature. To our knowledge, etching and coating are not often employed to treat Ti current collectors. The benefits from the mesh and foam structures for Ti current collectors are quite similar to that for Al and Cu current collectors.

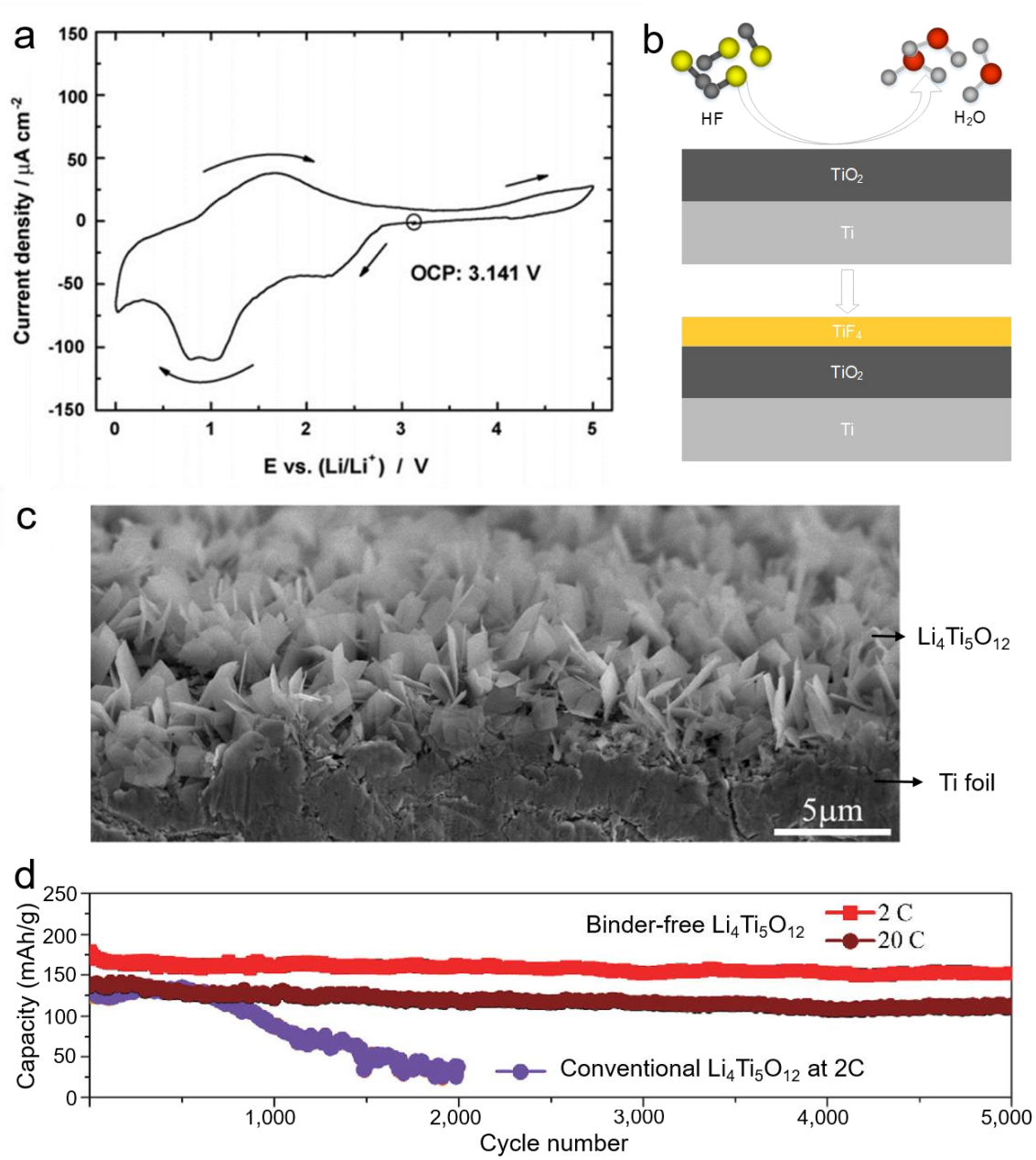

Fig. 5 a) Cyclic voltammetry of Ti in 1 M $LiPF_6$ in EC:DMC (1:1 vol.%) electrolyte (Reproduced with permission [30]. Copyright 2009 Elsevier), b) schematic drawing of passivation film formed on Ti surface, c) $Li_4Ti_5O_{12}$ nanoarrays grown on Ti foil (Reproduced with permission [160]. Copyright 2014 Royal Society of Chemistry), d) Long-life cycling performance of binder-free and conventional $Li_4Ti_5O_{12}$ anodes (Reproduced with permission [161]. Copyright 2014 Springer Nature).

Table. 4 Ti current collectors

Type	Electrode	Current rate/C	Capacity/ mAh g^{-1}	Capacity retention (cycles)	Reference
Foil	CoO	1	700	96% (20)	[150]
		2	500	93% (20)	
		4	375	83% (20)	
		6	200	75% (20)	
Foil	Co_3O_4	20	600	75% (20)	[151]
		50	400	60% (20)	
Foil	Co_3O_4	1.5	750	~100% (30)	[152]
		15	760	70% (30)	
		30	900	36% (30)	
Foil	Co_3O_4	200 [a]	964	~100% (100)	[153]
		5000 [a]	662	-	
Foil	Co_3O_4 and α-Fe_2O_3 composite	100 [a]	1200	82% (60)	[154]
Foil	SnO_2	0.2	980	71% (20)	[155]
		5	800	86% (20)	
		10	720	82% (20)	
Foil	SnO_2	200 [a]	550	~100% (30)	[156]
		1500 [a]	400	-	
Foil	α-Fe_2O_3	200 [a]	893	-	[157]
		500 [a]	814	112% (100)	
		10000 [a]	426	-	
Foil	TiO_2	0.2	266	~100% (50)	[158]
		10	66	-	
Foil	TiO_2	0.05	340	-	[159]
		2	125	-	
Foil	LTO	20	163	-	[160]
		50	145	86% (3000)	
		200	78	-	
Foil	LTO	2	174	88% (5000)	[161]
		20	139	83% (5000)	
		80	103	-	
Mesh	LMO	6.8	105	71% (1500)	[162]
Mesh	TiO_2	4.3 [a]	195	78% (100)	[163]

Mesh	TiO_2	10	267	-	[164]
		200	174	94% (6000)	
Mesh	LTO	1	188	-	[165]
		40	157	97% (325)	
		100	143	-	
Foam	TiO_2	0.11	387	~100% (100)	[166]
		5.61	312	-	
Foam	TiO_2	-	-	~100% (60)	[167]

[a] denotes a different unit of mA g^{-1} for current rate.

3.5 Stainless steel

3.5.1 Electrochemical stability

Stainless steel is an alloy mainly containing Fe, Cr, Ni and Mn, which is well known for high corrosion resistance due to the formation of a passivation film of chromium oxide on the surface [168]. The electrochemical behaviour of stainless steel (type 304) in 1 M $LiPF_6$ in EC/DMC 1:1 electrolyte is shown in Fig. 6a [44]. A cathodic peak between 1.5 and 2 V vs. Li/Li^+ is assumed to result from the reduction of the air-formed Fe- and/or Cr-oxide films, the electrolytic salt formation of Li_2O, and the formation of the SEI. Another cathodic peak occurs at about 0.6 V vs. Li/Li^+, which is an indicator of the underpotential deposition of Li on the stainless steel. No alloy between stainless steel and Li is formed as the potential approaches 0 V vs. Li/Li^+. In the anodic direction, deposited Li starts to oxidize at 1 V vs. Li/Li^+, generating an anodic peak current. As the applied potential increases to 2 V vs. Li/Li^+, another peak is observed due to the oxidation of Cr. A small anodic peak occurs at about 3.2 V vs. Li/Li^+, which is likely due to the oxidation of Fe and Cr^{3+}. Further increasing the applied potential up to 5 V results in very small current, implying that a stable passivation film is formed.

However, The passivation film is not strong enough to protect stainless steel against corrosion when used for $LiCoO_2$ and $LiMn_2O_4$ cathodes [169, 170]. Besides, the electrochemical stability of stainless steel at high potentials is also affected by Li salts. For example, stainless steel 304 is stable in 1 M $LiPF_6$ in EC/DEC electrolyte at potentials up to 4.5 V vs. Li/Li^+ but starts to react with the electrolyte of 1 M $LiClO_4$ in EC/DEC at 3 V vs Li/Li^+ [76]. Thus, the applicability of stainless steel current collectors for cathodes is questionable. On the other hand, the stable electrochemical behaviour at low potentials enables stainless steel to serve as current collectors for anodes.

The electrochemical stability is also sensitive to the composition of stainless steel. Fredriksson and Edström studied the electrochemical behaviour of duplex stainless steel LDX 2101 in 1 M $LiPF_6$ in EC/DMC 1:1 electrolyte [171]. Stainless steel LDX 2101 is known to have a higher content of Cr and N as well as a lower content of Ni than stainless steel 304, which results in stable electrochemical behaviour in a potential range of 3 – 4.5 V vs Li/Li^+. However, the stainless steel LDX 2101 is too reactive with the EC/DMC electrolyte. Fredriksson and Edström also proposed a three-layer structure of the passivation film on stainless steel LDX 2101, which is composed of a bottom layer of iron and chromium oxides, an interlayer of chromium hydroxide and a top layer of iron and chromium fluorides. The three-layer structure is also expected to be applicable for stainless steel 304.

3.5.2 Stainless steel current collector

Stainless steel (type 304) has a density of 7.9 g/cm^3, which is similar to Cu and Ni [48]. Stainless steel foils with a thickness of 25 μm have a tensile and yield strength of about 454 and 584 MPa [172], respectively, slightly higher than Cu foils. Adversely, stainless steel has a high electrical resistivity of 7.2×10^{-7} Ωm at room temperature [48], which is much higher than pure metals Cu, Al, Ni and Ti. The cost of stainless steel foils with a thickness of 25 μm is about $ 842 $/m^2$ (Goodfellow), which is similar to that of Cu and Ni foils.

Stainless steel is superior to other metals when used as current collectors for Fe contained anodes, e.g. α-Fe_2O_3 and $FeVO_4$. Li et al. directly fabricated α-Fe_2O_3 anodes on a stainless steel current collector via chemical corrosion in HCl and subsequent thermal oxidation [173]. The as-fabricated α-Fe_2O_3 anode delivers a capacity of 1105.6 mAh g^{-1} at 0.2 C after 200 cycles, which is even higher than the theoretical capacity, 1005 mAh g^{-1}. The stainless steel current collector serves as not only mechanical support for α-Fe_2O_3 anodes but also a source of Fe^{3+}. The direct fabrication of α-Fe_2O_3 on the stainless steel current collector provides firm adhesion and fast electron transport, avoiding the use of binder and carbon black. Similarly, Sim et al. directly fabricated $FeVO_4$ anodes on a stainless steel foil via chemical vapour deposition technique. The $FeVO_4$ anode exhibits a capacity of 1237 mAh g^{-1} at 0.15 C after 100 cycles, about 95% of the theoretical capacity [174].

Table 5 shows various stainless steel current collectors used for LIBs, including foil, mesh, coated and etched stainless steel. It is worth mentioning that all uncoated stainless steel current collectors are only used for anodes, which is indirect evidence that stainless steel may not be able to directly serve as a current collector for cathodes. With Au coating, stainless steel works perfectly for $Li(Ni_{0.5}Mn_{0.3}Co_{0.2})O_2$ and $LiCoO_2$ cathodes [175, 176]. Fig. 6c illustrates the synthesis procedure of the $LiCoO_2$ nanosheet arrays on an Au-coated stainless steel current collector. Apart from coating, a nitriding heat treatment was developed to treat stainless steel, which heats stainless steel at a temperature higher than 1200 ˚C in a nitrogen atmosphere. The nitrided stainless steel is stable at a potential higher than 5 V vs Li/Li^+ [177]. Overall, though stainless steel has been used as current collectors for many electrodes, the analysis of the advantages and disadvantages of stainless steel current collectors is scarce in the literature.

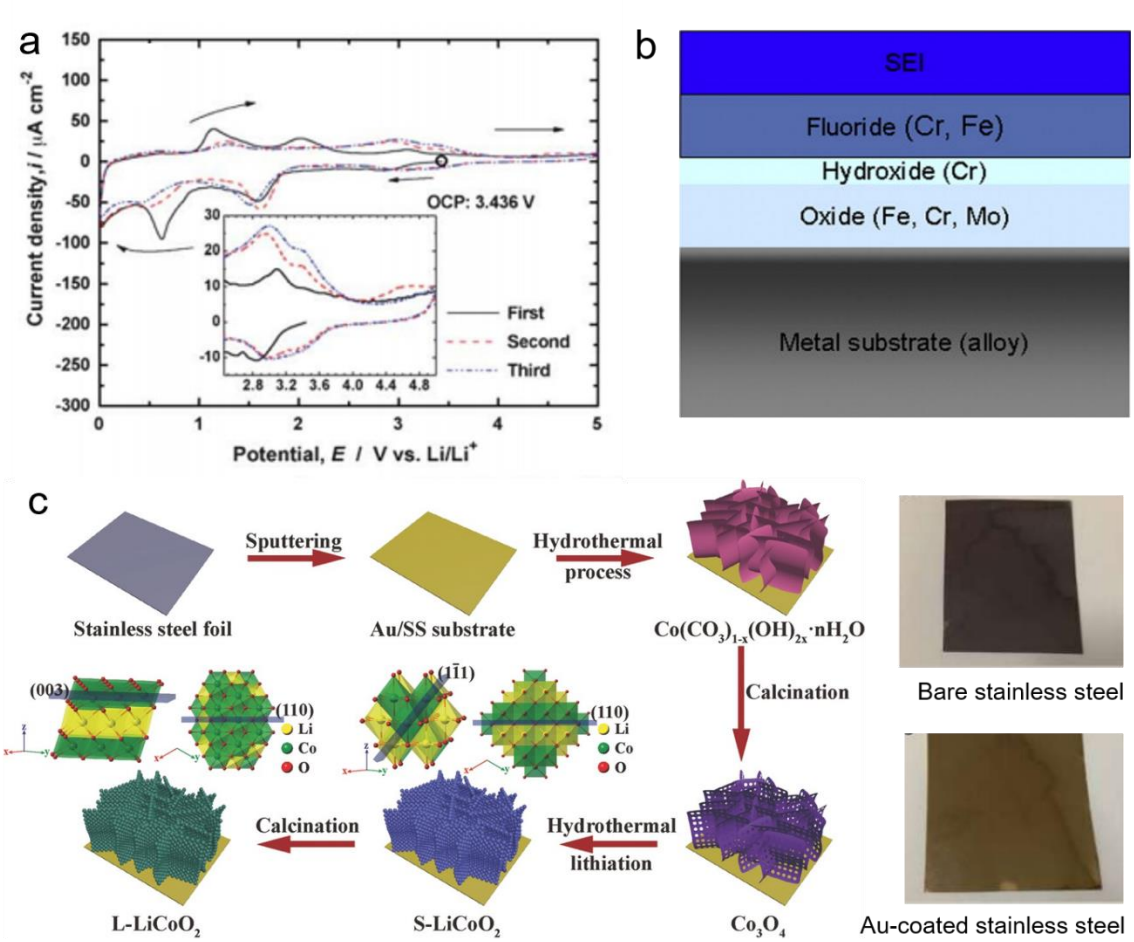

Fig. 6 a) Cyclic voltammetry of stainless steel (type 304) in 1 M $LiPF_6$ in EC:DMC (1:1 vol.%) electrolyte (Reproduced with permission [44]. Copyright 2011 Royal Society of

Chemistry), b) schematic drawing of passivation film formed on the surface of stainless steel (Reproduced with permission [171]. Copyright 2012 Elsevier), c) schematic illustration of the synthesis procedure of $LiCoO_2$ nanosheet arrays on Au-coated stainless steel, the right part is macrographs of a bare and an Au-coated stainless steel foil (Reproduced with permission [176]. Copyright 2018 John Wiley & Sons).

Table. 5 Stainless steel current collectors

Type	Electrode	Current rate/C	Capacity/ mAh g^{-1}	Capacity retention (cycles)	Reference
Foil	α-Fe_2O_3	0.2	858	129% (200)	[173]
		1	681	134% (500)	
		5	520	-	
Foil	$FeVO_4$	0.15	1316	94% (100)	[174]
		15	453	-	
Foil	Si	-	0.06 [c]	67% (70)	[178]
Foil	Si	0.2 [a]	0.55 [c]	-	[179]
Foil	Si	0.2	1600	72% (50)	[180]
Foil	Si	0.2	3800	84% (40)	[181]
		0.5	3600	86% (40)	
		1	3000	83% (40)	
Foil	SiO_2	0.005 [a]	646	~100% (250)	[182]
Foil	SnO_2 and a-Fe_2O_3 composite	0.1 [a]	1195	80% (50)	[183]
		0.3 [a]	600	78% (50)	
Foil	$CoFe_2O_4$	1	910	63% (100)	[184]
		2	900	59% (100)	
		4	810	56% (100)	
Foil	N-doped carbon	0.2	750	113% (150)	[185]
		2	415	-	
Foil	CoP	400 [b]	737	53% (900)	[186]
Foil	NiO	1	604	42% (100)	[187]
Foil	NiO and C composite	1	800	81% (100)	[187]
Foil	Co_3O_4	700 [b]	1000	60% (100)	[188]

Foil	Graphene and Co_3O_4 composite	700 [b]	1150	70% (100)	[188]
Foil	Co_3O_4	0.5	1200	42% (50)	[189]
Foil	ZnO	1	635	63% (100)	[190]
Mesh	Graphene oxide	50 [b]	530	60% (20)	[191]
		100 [b]	435	78% (20)	
Mesh	Co_3O_4	100 [b]	850	90% (80)	[192]
		800 [b]	625	-	
Mesh	Fe_2O_3 and $NiCo_2O_4$ composite	1000 [b]	650	90% (100)	[193]
Mesh	N-doped carbon	200 [b]	2058	-	[194]
		5000 [b]	313	-	
Au-coated	NMC532	0.5	125	89% (100)	[175]
Au-coated	LCO	0.1	130	82% (1000)	[176]
		10	105	-	
Au-coated	V_2O_5	0.33	265	~100% (20)	[195]
Etched	MnO_2	0.2	1300	107% (100)	[196]
		1	915	89% (95)	

[a] denotes a different unit of mA cm^{-2} for current rate.

[b] denotes a different unit of mA g^{-1} for current rate.

[c] denotes a different unit of mAh cm^{-2} for capacity.

3.6 Carbonaceous material

3.6.1 Electrochemical stability

Fig. 7a shows the electrochemical behaviour of fully-, semi-, non-graphitic carbon fibres and an Al foil in 1.2 M $LiPF_6$ in EC/DMC (1:2 vol.%) electrolyte [197]. The passivation film on the Al foil is expected to form after the 1st cycle. Before 4.5 V vs Li/Li^+, the currents generated at all carbon fibres are close to that of the Al foil at the 2nd cycle, indicating that all carbon fibres have good electrochemical stability. The current of all carbon fibres increases significantly after 4.5 V vs Li/Li^+ due to oxidation. It should be noted that the current in Fig. 7a is normalised by the geometric surface area. Considering that the carbon fibres have much higher electroactive surface areas, i.e. the surface area where chemical reactions take place, than the Al foil, the real areal current densities on the carbon fibres should be much lower than that of the Al

foil, indicating better electrochemical stability. Additionally, carbonaceous materials have been widely used as conductive additives, e.g. carbon black, and even anodes, e.g. graphite and graphene in LIBs [198], indicating good electrochemical stability at a wide potential range. Thus, carbonaceous materials can serve as current collectors for both cathodes and anodes.

3.6.2 Carbonaceous current collector

Carbonaceous current collectors, e.g. carbon fibre papers, are superior to metal current collectors in many aspects. Firstly, carbonaceous current collectors are favourable to increasing the ratio of active to non-active material at electrodes. Carbon fibre papers with a porosity of 78% have a density of 0.44 g/cm^3 [199], which is one order of magnitude lower than that of metal foils. Besides, the porous structure allows several times higher mass loading than planar metal current collectors and thus higher gravimetric capacity [200, 201]. Secondly, carbonaceous substrates for anodes not only serve as current collectors but also participate in lithiation/delithiation processes as active materials, which further contribute to high battery capacity. Shafiei and Alpas coated Sn anodes on a carbon fibre paper which serves as both a current collector and active material [202]. The Sn-coated carbon fibre delivers an initial discharge capacity of about 3 mAh cm^{-2}, almost four times higher than that of a Sn anode on a Cu foil current collector. Thirdly, carbonaceous current collectors have unique mechanical properties. The tensile strength of carbon fibre paper, with a mass fraction of carbon fibre in the range of 0 – 50%, is up to 5 MPa [203]. Unlike metal current collectors that easily undergo plastic deformation, carbonaceous current collectors can be folded multiple times without plastic deformation, which is an ideal material for future flexible LIBs [204]. Fig. 7b-d shows a flexible $Li_4Ti_5O_{12}$ anode on a carbon fibre paper current collector, which delivers a capacity higher than 150 mAh g^{-1} after repeated bending [205]. A similar study for developing flexible current collectors based on carbonaceous materials can be found in [206]. Fourthly, carbonaceous current collectors can improve electron and ion transfer kinetics. Though carbon fibre papers have a relatively high electrical resistance of 8 x 10^{-4} Ωm [199], the porous structures of carbonaceous current collectors provide high contact area between electrodes and current collectors as well as pathways for Li-ion diffusion, lowering interfacial resistance and increasing mass transfer kinetics [207-210]. Additionally, the flexible structure of carbonaceous materials can effectively alleviate strain and stress caused

by battery cycling, maintaining good current collector/electrode contact and thus high conductivity. Last but not least, carbonaceous current collectors are cheaper than metal current collectors. According to the online quotation from Goodfellow, carbon fabric with a thickness of 0.15 mm costs $ 440 /m^2, which is equivalent for $ 60 /m^2 for carbon fabric with a thickness of 20 μm.

In addition to carbon fibre papers, many other carbonaceous materials have also been used as current collectors for LIBs; carbon foams, carbon nanotubes, carbon nanofibres and graphene foams. Chu et al. fabricated carbon foams with an average pore size of 39 nm and a BET surface area about 350 m^2/g by the carbonization of melamine foams at a high temperature of 800 ºC and subsequent punching [211]. Nanosized TiO_2 anode was deposited on the as-fabricated carbon foam current collectors, which exhibits a capacity of 203 and 104 mAh g^{-1} at 0.3 and 6 C, respectively. Carbon foam current collectors have also been fabricated by the carbonization of melamine or PVDF for silicon anodes in other studies [212, 213]. A 10-layer carbon nanotube current collector with an extremely low density of 2 mg/cm^3 has been fabricated for silicon anodes [214]. The silicon anode on the carbon nanotube current collector delivers a high capacity of about 1600 mAh g^{-1} at 100 mA g^{-1} and remains at 94% after 45 cycles. Besides this, the carbon nanotube current collector has also been used in the development of flexible LIBs [215-217]. Kim developed a 3D Si/carbon nanofibre anode by electrospinning [218]. Though the authors described the anode as current collector-free, carbon nanofibres serve as a mechanical support and current collector for silicon nanoparticles. The silicon anode exhibited a high initial capacity of 1957 mAh g^{-1} at 2 A g^{-1} and maintained at about 60% after 400 cycles. Carbon nanofibre current collectors with ultrafine titanium nitride sheath decoration have also been used for Li metal anodes to alleviate the formation of Li dendrites [219]. Chao and his colleagues directly fabricated V_2O_5 nanoarrays cathode on a graphene foam (also named ‘ultrathin graphite foam’ in some publications) via a solvothermal synthesis process [220]. The graphene foam has an ultrahigh porosity of 99.7% and an electrical resistance of 10^{-3} Ωm which is similar to carbon fibre papers, serving as a current collector. The V_2O_5 cathode on the graphene foam delivers a capacity of 265 and 168 mAh g^{-1} at 5 and 60 C, respectively. The capacity remains at 98% at 60 C after 1000 cycles. Many other studies on graphene foam current collectors have been reported in [221-223].

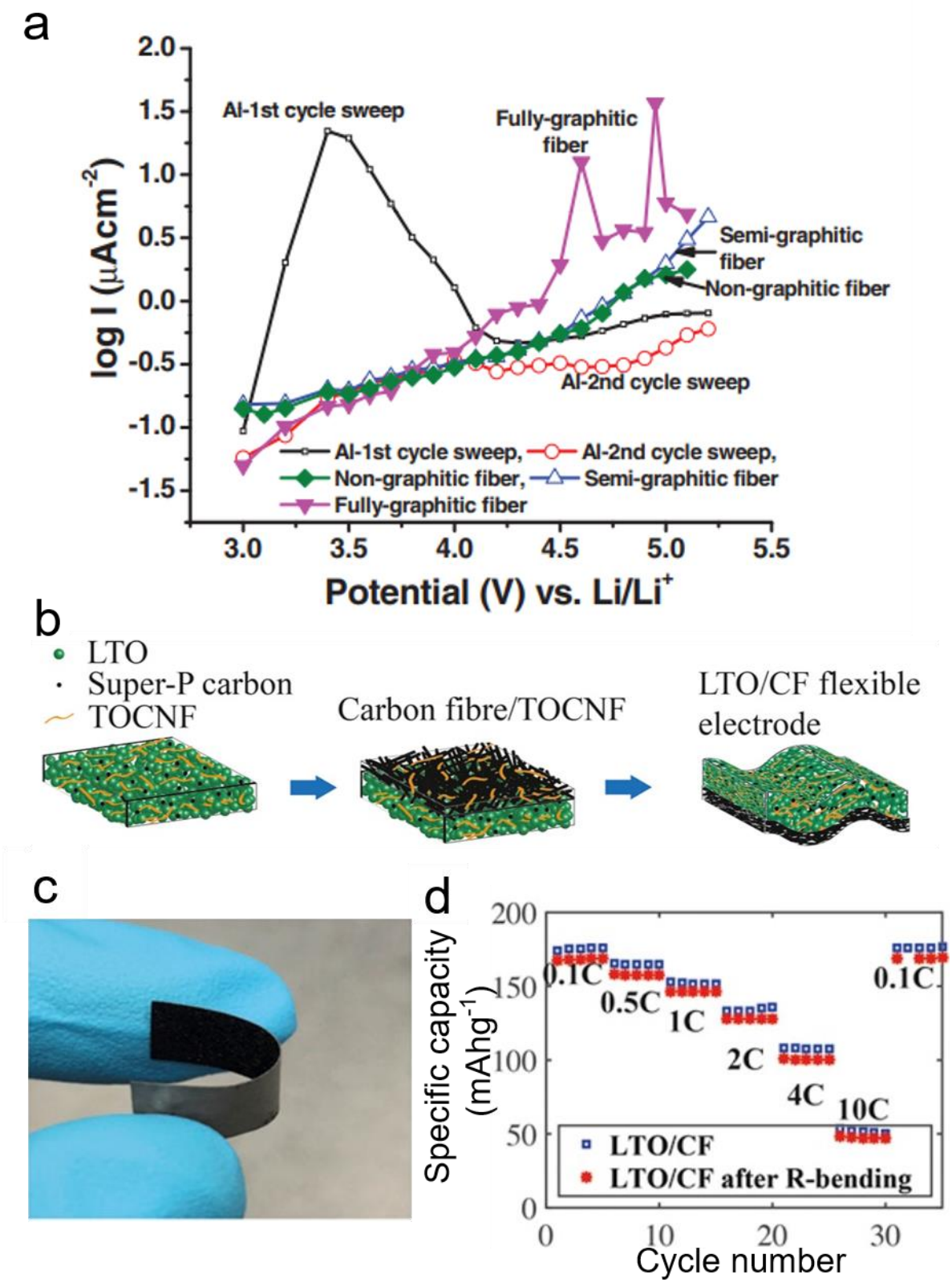

Fig. 7 a) Cyclic voltammetry of fully-, semi-, non-graphitic carbon fibres and Al foil in 1.2 M $LiPF_6$ in EC/DMC (1:2 vol.%) electrolyte (Reproduced with permission [197]. Copyright 2012 IOP Publishing), b) preparation of $Li_4Ti_5O_{12}$ anode on carbon fibre (CF)

current collector, with super-b carbon black and TEMPO oxidized cellulose nanofibrils (TOCNF) as a binder, c) macrograph of the flexible $Li_4Ti_5O_{12}$ anode on a carbon fibre current collector, d) capacity vs. cycle number measured at different rates of the $Li_4Ti_5O_{12}$ anode before and after repeat bending (R-bending) (Reproduced with permission [205]. Copyright 2017 Elsevier).

Table. 6 Carbonaceous current collectors

Type	Electrode(s)	Current rate/C	Capacity/ mAh g^{-1}	Capacity retention (cycles)	Reference
CFP	Si	0.1	1800	75% (40)	[200]
CFP	Si	0.1	700	93% (100)	[201]
CFP	Sn	1.5 [a]	152	50% (20)	[202]
CFP	LTO	0.1	166	-	[205]
		2	124	83% (100)	
		10	50	-	
CFP	LFP	0.1	150	-	[206]
		1	133	-	
CFP	Si and reduced graphene oxide composite	0.1	1100	-	[208]
		2.5	550	95% (100)	
		10	280	-	
CFP	Si	1	700	98% (10)	[209]
CFP	LVP and carbon composite	0.5	122	-	[210]
		10	108	95% (1000)	
		1	97.4	-	
CF	TiO_2	0.3	203	-	[211]
		3	150	75% (100)	
		6	104	-	
CF	Si	2000 [b]	1500	86% (1000)	[212]
CF	Si	0.05	2200	81% (123)	[213]
		0.1	2200	61% (142)	
		0.2	2040	69%(112)	
CNT	Si	50 [b]	1720	-	[214]
		100 [b]	1590	94% (45)	

		800 [b]	100	-	
CNT	LTO	1	153	93% (200)	[215]
CNT	LTO	0.25	132	~100% (80)	[216]
CNT	LCO	0.25	134	93% (80)	[216]
CNT	LTO	10 [b]	160	94% (350)	[217]
CNF	Si	2000 [b]	1957	61% (400)	[218]
CNF	Li/LFP	1	160	78% (250)	[219]
GF	V_2O_5	5	265	~100% (500)	[220]
		60	168	98% (1000)	
GF	Ge	1	1220	96%(1000)	[221]
		40	800	-	
GF	FeS_2	0.2	1250	86% (100)	[222]
GF	Li/LFP	0.5	160	88% (100)	[223]
		2	106	-	

Note: CFP, CF, CNT, CNF and GF stands for carbon fibre paper, carbon foam, carbon nanotube, carbon nanofibre and graphene foam, respectively.

[a] denotes a different unit of mA cm^{-2} for current rate.

[b] denotes a different unit of mA g^{-1} for current rate.

4. Summary

4.1 Comparison of materials

Fig. 8a compares the performance of all materials reviewed in this work in five aspects. Carbon fibre paper is used to represent carbonaceous materials in comparison. In terms of electrochemical stability, Ti and carbon fibre have the largest stable potential range of 0 – 5 V vs. Li/Li^+, allowing them to be employed as current collectors for both cathodes and anodes. Al has a relatively large stable potential range of ~0.5 – 5 V vs. Li/Li^+ because the alloying reaction of Al and Li takes place at potentials close to 0 V vs. Li/Li^+. Cu and Ni are stable at potentials up to 3.5 V vs. Li/Li^+. Stainless steel has the smallest stable potential range of 0 – 3 V vs. Li/Li^+. Thus, Cu, Ni and stainless steel can be used as current collectors for anodes only.

The second criterion is electrical conductivity. Cu has the lowest resistivity of 1.68 x 10^{-8} Ωm, followed by Al (2.65 x 10^{-8} Ωm), Ni (6.93 x 10^{-8} Ωm), Ti (3.9 x 10^{-7} Ωm), stainless steel (7.2 x 10^{-7} Ωm) and carbon fibre paper (8 x 10^{-4} Ωm). A common query about the performance of Al current collectors is the effect of the air-formed Al_2O_3 layer

on the electrical conductivity. Comparing the theoretical electrical conductivity of pure Al and the measured electrical conductivity of untreated Al wires and rods shows that the Al_2O_3 layer does not affect the electrical conductivity of Al current collectors. It is generally accepted that other metals and carbon-based materials are stable under the exposure of air. To the best of our knowledge, very little work has been done on the effect of passivation films on the electrical conductivity of current collectors. The contact resistance between the current collector and electrode is much higher than the resistance of the current collector itself and there has been much work in modifying the surface to improve adhesion and through-plane conductivity. It is necessary to minimise the contact resistance to improve the overall conductivity in practical applications.

In terms of tensile strength, the order of the metal foils from high to low, is Ni (730 MPa), stainless steel (454 MPa), Ti (360 MPa), Cu (~325 MPa) and Al (25 MPa). Carbon fibre papers have a tensile strength lower than 5 MPa. Advantageously, the soft structure makes carbon fibre paper an ideal choice for flexible current collectors.

When it comes to density, carbon fibre papers are the lightest material with a density of about 0.44 g/cm^3, followed by Al (2.7 g/cm^3), Ti (4.51 g/cm^3), stainless steel (7.9 g/cm^3), Ni (8.9 g/cm^3) and Cu (8.96 g/cm^3). As the conventional Cu current collector takes up 13% of the total weight of a LIB, assuming other conditions are the same, replacing the Cu foil with an identically sized carbon fibre paper as the current collector is expected to reduce the total weight of the LIB by 12% and thus increase the gravimetric capacity by 14%.

Last but not least, the cost and sustainability vary with materials greatly. Based on the online quotation from Goodfellow in June 2020, the order of the six types of foils in cost, from low to high, is carbon fabric ($ 60 /m^2), Al ($ 130 /m^2), Cu ($ 640 /m^2), Ni ($ 795 /m^2), stainless steel ($ 842 /m^2) and Ti ($ 3100 /m^2). All of the foils have similar thicknesses around 20 μm and purity higher than 99%. In terms of sustainability, carbon is the most abundant material among the six materials, followed by Al, stainless steel (based on Fe reserve), Ti, Ni and Cu [224, 225]. Recyclability is an important part of sustainability. It is reported that Al and Cu foils can be easily separated from electrode active materials by ultrasonic treatments or heating and then recycled or

reused [226-228]. However, the recyclability of other materials has not been well investigated.

4.2 Effects of structures and treatments

Current collectors are normally employed in the forms of foil, mesh and foam. Foil is the simplest structure which is easy to produce and process. However, the mediocre performance of foil current collectors makes it is difficult to meet the requirements for next-generation LIBs. Mesh current collectors are expected to improve electrode performance due to increased surface area and enhanced charge transfer kinetics. The limitation is that mesh current collectors have low mechanical strength. Foam current collectors can provide even higher surface area than mesh current collectors. Besides, the porous structure also allows high mass loading, efficient Li-ion diffusion, fast charge transfer and accommodation of electrode volume change during cycling, greatly improving electrode performance. It also should be noted that the electrode loading technique is crucial when using mesh and foam current collectors. For example, a large amount of active material can be loaded evenly on foam current collectors by electrodeposition, thus enhancing performance, while very limited active material can be loaded via dip-coating, causing a huge waste of useful surface area.

Chemical etching and coating are two commonly used treatments for current collectors. Chemical etching can effectively roughen the surface of current collectors, which is favourable for improving adhesion and interfacial conductivity between electrodes and current collectors as well as electrode/electrolyte charge transfer kinetics. Current collectors with patterns for particular purposes can be fabricated by selective etching to alleviate the volume change of some specific anodes. Nevertheless, chemical etching may also bring a risk of contamination and reduce the mechanical strength of current collectors. Coating is an effective way to change the surface material to achieve better performance. The coated material can improve the electrochemical stability, charge transfer property, interfacial adhesion and conductivity of current collectors. Besides, current collectors coated with lithiophilic materials, e.g. CuO and Ag, can reduce the nucleation overpotential and guide uniform Li nucleation and deposition, effectively preventing the formation of Li dendrites.

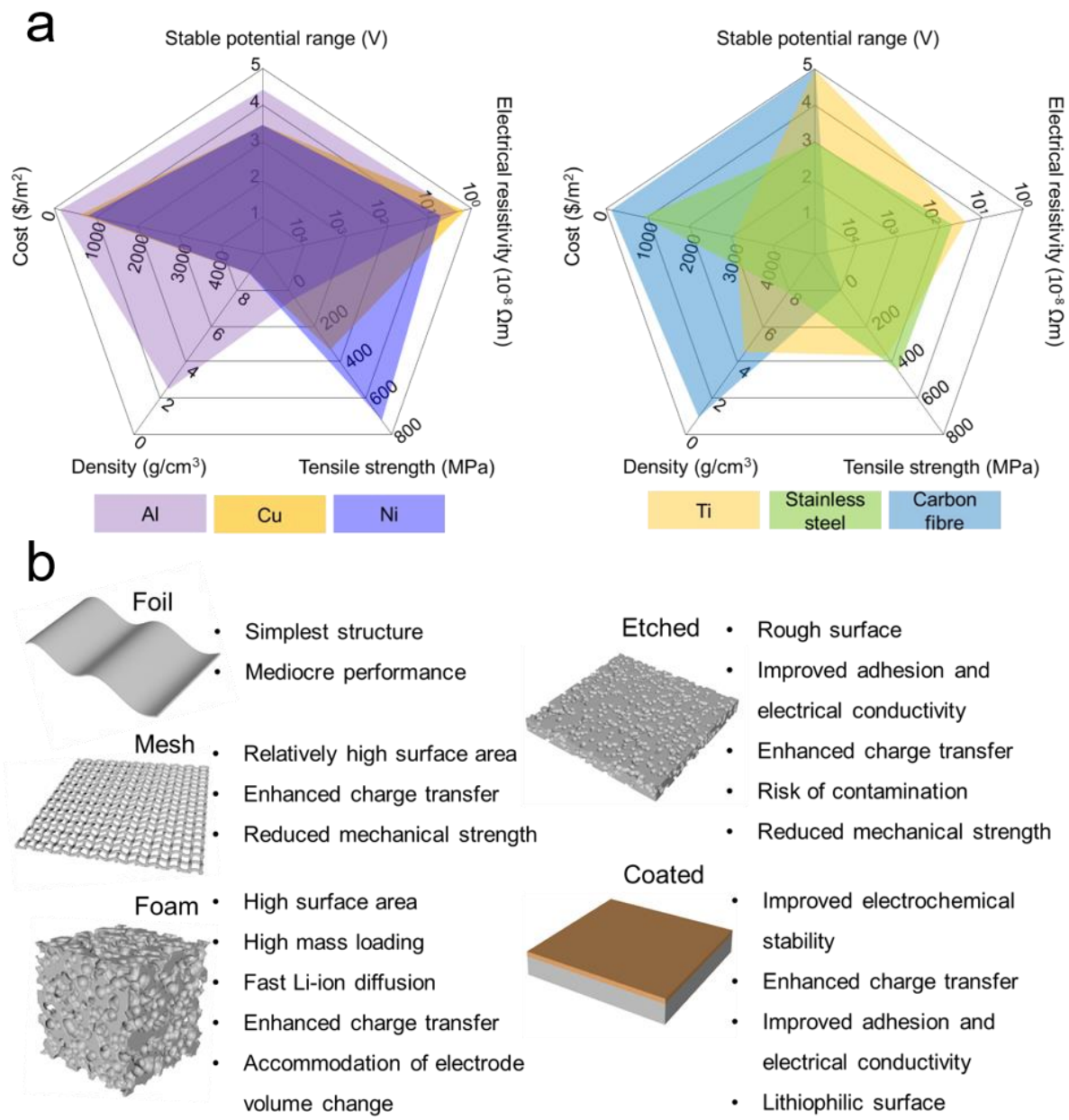

Fig. 8 a) Comparison of Al, Cu, Ni, Ti, stainless steel and carbon fibre in five aspects of stable potential range, electrical resistivity, tensile strength, density and cost; b) main advantages and disadvantages of current collectors with three different structures of foil, mesh and foam, as well as two treatments of chemical etching and coating. Note: the carbon fabric with a thickness of 0.15 mm costs $ 440 /m^2, which is equivalent for $ 60 /m^2 for carbon fabric with a thickness of 20 μm.

4.3 Future directions

The development of next-generation LIBs will go in the direction of higher capacity, longer service lifetime, more environmental-friendliness and lower cost, which requires

potential current collectors to be more electrochemically stable, more conductive, lighter and cheaper. Additionally, current collectors with flexible structures are also necessary for the applications of future wearable devices. To achieve this goal, further efforts should be made on the following topics.

- Carbonaceous materials have been regarded as a promising alternative to conventional Al and Cu current collectors in the literature. However, the use of carbonaceous materials in real LIBs is still problematic due to low weldability. At present, all metallic current collectors are connected with electrode tabs by welding, providing a good bonding and electrical contact. However, It is very hard to weld carbonaceous materials due to the extremely high temperature and pressure needed for melting [229]. Therefore, more efforts should be made on securing good contacts between the carbonaceous current collectors and electrode tabs.
- Porous current collectors are ideal choices for high electrode mass loading [230, 231]. On the one hand, the enhanced mass loading can improve absolute LIB capacity. On the other hand, the enhanced mass loading may sacrifice gravimetric capacity due to increased internal electrical resistance and limited Li-ion diffusion [98]. We need to optimise the porous structure of current collectors, e.g. porosity, pore size and pore shape, to increase electrode mass loading as well as keep electrical resistance low and Li-ion diffusion rate high. So we can improve both absolute and gravimetric capacity of LIBs at the same time.
- Polymers have lower densities than metals and better mechanical strength than carbonaceous material, which is a potential material for current collectors [232]. In addition, polymers are expected to have better corrosion resistance than conventional metal current collectors. Nevertheless, low electrical conductivity is a major obstacle for polymeric current collectors. The electrical conductivity of polymeric current collectors needs further improvement to meet the requirements for high power LIBs. Another concern is the thermal conductivity and stability. Metallic current collectors transfer heat in addition to electrons. Future polymeric current collectors need similar high thermal conductivities to avoid heat accumulation in LIBs and provide thermal stability in the normal operating temperature range.
- Surface coating is a commonly used treatment to make current collectors more stable, conductive and improve adhesion properties. Thick coatings can add extra

weight to LIBs, while thin coatings may result in insufficient protection and conduction [70]. A uniform coating layer with an appropriate thickness is beneficial for high LIB performance. Thus, the coating thickness and uniformity need to be precisely controlled. Besides, the coating material is also an important factor. Current collectors coated with lighter and more conductive materials are desirable for the next generation LIBs.

- Recycling or reusing conventional current collectors can not only protect our environment but also provide a secondary source of some valuable materials, reducing the cost of current collectors [29]. To our knowledge, although the strategy for the recycling of Al and Cu foils from end-of-life LIBs has been proposed in many studies [226-228], subsequent characterisation and testing of the recycled Al and Cu foils have not been well reported. Whether the recycled Al and Cu current collectors can be directly reused in new LIBs is still unknown. Furthermore, knowledge about the recyclability of other current collectors is still lacking and needs investigating.

Abbreviation

CMC	Carboxymethyl cellulose
DG	Diglyme
EC	Ethylene carbonate
EMC	Ethyl methyl carbonate
DEC	Diethyl carbonate
DMC	Dimethyl carbonate
LCO	Lithium cobalt oxide, $LiCoO_2$
LFP	Lithium iron phosphate, $LiFePO_4$
LMO	Lithium manganese oxide, $LiMn_2O_4$
LNMO	Lithium nickel manganese oxide, $LiNi_{0.5}Mn_{1.5}O_4$
NMC	Lithium nickel manganese cobalt oxide, $LiNiMnCoO_2$
LTO	Lithium titanate oxide, $Li_4Ti_5O_{12}$
LVP	Lithium vanadium phosphate, $Li_3V_2(PO_4)_3$
MFA	Methyl difluoroacetate
PC	Propylene carbonate
β-PVDF	β-phase polyvinylidene difluoride

CRediT authorship contribution statement

Pengcheng Zhu: Conceptualization, Investigation, Writing - original draft preparation, **Emma Kendrick** and **Vannessa Goodshipa:** Conceptualization,

Funding acquisition, Project administration, **Dominika Gastol**, **Jean Marshall** and **Roberto Sommerville:** Investigation, Writing - Review & Editing.

Declaration of competing interest

The authors declare that they have no known competing financial interests or personal relationships that could have appeared to influence the work reported in this paper.

Funding

This research was funded by the Faraday Institution; ReLiB fast-start project (grant numbers FIRG005 and FIRG006), the Innovate UK though the Faraday Challenge; R2LIB, TS/S004572/1.

Reference

[1] J.-M. Tarascon, M. Armand, nature, 414 (2001) 359-367.
[2] J.B. Goodenough, Y. Kim, Chemistry of materials, 22 (2010) 587-603.
[3] L. Lu, X. Han, J. Li, J. Hua, M. Ouyang, Journal of power sources, 226 (2013) 272-288.
[4] S. Pacala, R. Socolow, science, 305 (2004) 968-972.
[5] I. Rubio Lopez, M.J. Lain, E. Kendrick, Batteries & Supercaps, (2020).
[6] A. Jaiswal, Renewable and Sustainable Energy Reviews, 72 (2017) 922-934.
[7] S.B. Chikkannanavar, D.M. Bernardi, L. Liu, Journal of Power Sources, 248 (2014) 91-100.
[8] S. Goriparti, E. Miele, F. De Angelis, E. Di Fabrizio, R.P. Zaccaria, C. Capiglia, Journal of power sources, 257 (2014) 421-443.
[9] C.-H. Chen, F.B. Planella, K. O'Regan, D. Gastol, W.D. Widanage, E. Kendrick, Journal of The Electrochemical Society, 167 (2020) 080534.
[10] M. Marcinek, J. Syzdek, M. Marczewski, M. Piszcz, L. Niedzicki, M. Kalita, A. Plewa-Marczewska, A. Bitner, P. Wieczorek, T. Trzeciak, Solid State Ionics, 276 (2015) 107-126.
[11] X. Huang, Journal of Solid State Electrochemistry, 15 (2011) 649-662.
[12] J.T. Warner, The handbook of lithium-ion battery pack design: chemistry, components, types and terminology, Elsevier, 2015.
[13] B.A. Johnson, R.E. White, Journal of power sources, 70 (1998) 48-54.
[14] L.-P. He, S.-Y. Sun, X.-F. Song, J.-G. Yu, Waste management, 46 (2015) 523-528.
[15] C.C. Wang, Y.C. Lin, K.F. Chiu, H.J. Leu, T.H. Ko, ChemistrySelect, 2 (2017) 4419-4427.
[16] M.J. Lain, J. Brandon, E. Kendrick, Batteries, 5 (2019) 64.
[17] S. Jin, Y. Jiang, H. Ji, Y. Yu, Advanced Materials, 30 (2018) 1802014.
[18] M. Yamada, T. Watanabe, T. Gunji, J. Wu, F. Matsumoto, Electrochem, 1 (2020) 124-159.
[19] M. Li, J. Lu, Z. Chen, K. Amine, Advanced Materials, 30 (2018) 1800561.
[20] S. Murashige, N. Arai, in, Google Patents, 2004.
[21] J.B. Goodenough, Accounts of chemical research, 46 (2013) 1053-1061.
[22] C. Liu, Z.G. Neale, G. Cao, Materials Today, 19 (2016) 109-123.
[23] S.J. An, J. Li, C. Daniel, D. Mohanty, S. Nagpure, D.L. Wood III, Carbon, 105 (2016) 52-76.
[24] S. Zhang, T. Jow, Journal of Power Sources, 109 (2002) 458-464.

[25] P.S. Kumar, S. Ayyasamy, E.S. Tok, S. Adams, M. Reddy, ACS omega, 3 (2018) 3036-3044.
[26] A. Kraytsberg, Y. Ein‐Eli, Advanced Energy Materials, 6 (2016) 1600655.
[27] D. Ma, Z. Cao, A. Hu, Nano-Micro Letters, 6 (2014) 347-358.
[28] J. Li, Z. Du, R.E. Ruther, S.J. An, L.A. David, K. Hays, M. Wood, N.D. Phillip, Y. Sheng, C. Mao, Jom, 69 (2017) 1484-1496.
[29] G. Harper, R. Sommerville, E. Kendrick, L. Driscoll, P. Slater, R. Stolkin, A. Walton, P. Christensen, O. Heidrich, S. Lambert, Nature, 575 (2019) 75-86.
[30] S.-T. Myung, Y. Sasaki, S. Sakurada, Y.-K. Sun, H. Yashiro, Electrochimica Acta, 55 (2009) 288-297.
[31] K. Kanamura, T. Okagawa, Z.-i. Takehara, Journal of power sources, 57 (1995) 119-123.
[32] X. Zhang, T. Devine, Journal of The Electrochemical Society, 153 (2006) B344-B351.
[33] X. Zhang, T. Devine, Journal of The Electrochemical Society, 153 (2006) B375-B383.
[34] J.W. Braithwaite, A. Gonzales, G. Nagasubramanian, S.J. Lucero, D.E. Peebles, J.A. Ohlhausen, W.R. Cieslak, Journal of the electrochemical society, 146 (1999) 448.
[35] S. Wiemers-Meyer, S. Jeremias, M. Winter, S. Nowak, Electrochimica Acta, 222 (2016) 1267-1271.
[36] X. Zhang, T.M. Devine, Journal of The Electrochemical Society, 153 (2006) B365-B369.
[37] H. Yang, K. Kwon, T.M. Devine, J.W. Evans, Journal of The Electrochemical Society, 147 (2000) 4399-4407.
[38] M. Morita, T. Shibata, N. Yoshimoto, M. Ishikawa, Electrochimica Acta, 47 (2002) 2787-2793.
[39] X. Chen, W. Xu, M.H. Engelhard, J. Zheng, Y. Zhang, F. Ding, J. Qian, J.-G. Zhang, Journal of Materials Chemistry A, 2 (2014) 2346-2352.
[40] K. Park, S. Yu, C. Lee, H. Lee, Journal of Power Sources, 296 (2015) 197-203.
[41] S. Theivaprakasam, G. Girard, P. Howlett, M. Forsyth, S. Mitra, D. MacFarlane, NPJ Materials Degradation, 2 (2018) 1-9.
[42] L. Zhang, L. Chai, L. Zhang, M. Shen, X. Zhang, V.S. Battaglia, T. Stephenson, H. Zheng, Electrochimica Acta, 127 (2014) 39-44.
[43] S.-W. Song, T.J. Richardson, G.V. Zhuang, T.M. Devine, J.W. Evans, Electrochimica acta, 49 (2004) 1483-1490.
[44] S.-T. Myung, Y. Hitoshi, Y.-K. Sun, Journal of Materials Chemistry, 21 (2011) 9891-9911.
[45] T. Kawamura, T. Tanaka, M. Egashira, I. Watanabe, S. Okada, J.-i. Yamaki, Electrochemical and Solid-State Letters, 8 (2005) A459-A463.
[46] G. Xu, P. Han, S. Dong, H. Liu, G. Cui, L. Chen, Coordination Chemistry Reviews, 343 (2017) 139-184.
[47] A. Yoshino, K. Sanechika, T. Nakajima, in, Google Patents, 1987.
[48] W. Haynes, C. Handbook, in, CRC Press, 2016.
[49] L. Tian, A. Russell, T. Riedemann, S. Mueller, I. Anderson, Materials Science and Engineering: A, 690 (2017) 348-354.
[50] R. Brandt, G. Neuer, International Journal of Thermophysics, 28 (2007) 1429-1446.
[51] P.A. Nelson, K.G. Gallagher, I.D. Bloom, D.W. Dees, in, Argonne National Lab.(ANL), Argonne, IL (United States), 2012.
[52] M. Lederer, V. Gröger, G. Khatibi, B. Weiss, Materials Science and Engineering: A, 527 (2010) 590-599.
[53] P. Arora, M. Doyle, A.S. Gozdz, R.E. White, J. Newman, Journal of power Sources, 88 (2000) 219-231.
[54] R.A. Hikmet, Journal of power sources, 92 (2001) 212-220.
[55] K. Kanamura, W. Hoshikawa, T. Umegaki, Journal of the Electrochemical Society, 149 (2002) A339-A345.
[56] S. Venkatraman, V. Subramanian, S.G. Kumar, N. Renganathan, N. Muniyandi, Electrochemistry communications, 2 (2000) 18-22.
[57] X. Wang, H. Hao, J. Liu, T. Huang, A. Yu, Electrochimica acta, 56 (2011) 4065-4069.
[58] S. Ramesh, K. Ramesh, A. Arof, Int J Electrochem Sci, 8 (2013) 8348-8355.

[59] M. Herklotz, F. Scheiba, R. Glaum, E. Mosymow, S. Oswald, J. Eckert, H. Ehrenberg, Electrochimica Acta, 139 (2014) 356-364.
[60] M. Fritsch, G. Standke, C. Heubner, U. Langklotz, A. Michaelis, Journal of Energy Storage, 16 (2018) 125-132.
[61] K.G. Gallagher, S.E. Trask, C. Bauer, T. Woehrle, S.F. Lux, M. Tschech, P. Lamp, B.J. Polzin, S. Ha, B. Long, Journal of The Electrochemical Society, 163 (2016) A138-A149.
[62] H. Zheng, J. Li, X. Song, G. Liu, V.S. Battaglia, Electrochimica Acta, 71 (2012) 258-265.
[63] X. Du, Q. Wang, T. Feng, X. Chen, L. Li, L. Li, X. Meng, L. Xiong, X. Sun, L. Lu, Scientific reports, 6 (2016) 20138.
[64] T. Nakamura, S. Okano, N. Yaguma, Y. Morinaga, H. Takahara, Y. Yamada, Journal of power sources, 244 (2013) 532-537.
[65] S. Yoon, H.-S. Jang, S. Kim, J. Kim, K.Y. Cho, Journal of Electroanalytical Chemistry, 797 (2017) 37-41.
[66] S. Nakanishi, T. Suzuki, C. Qi, J. Akikusa, K. Nakamura, Transactions of Nonferrous Metals Society of China, 24 (2014) 2314-2319.
[67] D.-Y. Shin, D.-H. Park, H.-J. Ahn, Applied Surface Science, 475 (2019) 519-523.
[68] K. Striebel, J. Shim, A. Sierra, H. Yang, X. Song, R. Kostecki, K. McCarthy, Journal of Power Sources, 146 (2005) 33-38.
[69] H.-C. Wu, E. Lee, N.-L. Wu, T.R. Jow, Journal of power sources, 197 (2012) 301-304.
[70] I. Doberdò, N. Löffler, N. Laszczynski, D. Cericola, N. Penazzi, S. Bodoardo, G.-T. Kim, S. Passerini, Journal of power sources, 248 (2014) 1000-1006.
[71] S.R. Prabakar, Y.-H. Hwang, E.G. Bae, D.K. Lee, M. Pyo, Carbon, 52 (2013) 128-136.
[72] S. Kang, H. Xie, W. Zhai, Z. Ma, R. Wang, W. Zhang, Int. J. Electrochem. Sci, 10 (2015) 2324-2335.
[73] S. Gheytani, Y. Liang, Y. Jing, J.Q. Xu, Y. Yao, Journal of Materials Chemistry A, 4 (2016) 395-399.
[74] S.Y. Kim, Y.I. Song, J.-H. Wee, C.H. Kim, B.W. Ahn, J.W. Lee, S.J. Shu, M. Terrones, Y.A. Kim, C.-M. Yang, Carbon, 153 (2019) 495-503.
[75] H. Lee, J.-J. Cho, J. Kim, H.-J. Kim, Journal of the Electrochemical Society, 152 (2005) A1193-A1198.
[76] C. Iwakura, Y. Fukumoto, H. Inoue, S. Ohashi, S. Kobayashi, H. Tada, M. Abe, Journal of power sources, 68 (1997) 301-303.
[77] J. Kawakita, K. Kobayashi, Journal of power sources, 101 (2001) 47-52.
[78] M. Zhao, S. Kariuki, H.D. Dewald, F.R. Lemke, R.J. Staniewicz, E.J. Plichta, R.A. Marsh, Journal of the Electrochemical Society, 147 (2000) 2874-2879.
[79] S. Dai, J. Chen, Y. Ren, Z. Liu, J. Chen, C. Li, X. Zhang, X. Zhang, T. Zeng, Int. J. Electrochem. Sci, 12 (2017) 10.
[80] R. Guo, L. Lu, M. Ouyang, X. Feng, Scientific reports, 6 (2016) 30248.
[81] K. Shinozaki, A. Suzuki, T. Tsuruta, in, Google Patents, 2012.
[82] J.-M. Song, Y.-S. Zou, C.-C. Kuo, S.-C. Lin, Corrosion science, 74 (2013) 223-231.
[83] M. Guo, W. Meng, X. Zhang, Z. Bai, G. Wang, Z. Wang, F. Yang, Journal of Electronic Materials, 48 (2019) 7543-7550.
[84] J. Zhu, J. Feng, Z. Guo, RSC advances, 4 (2014) 57671-57678.
[85] Q. Li, S. Zhu, Y. Lu, Advanced Functional Materials, 27 (2017) 1606422.
[86] H.-Y. Lee, S.-M. Lee, Electrochemistry Communications, 6 (2004) 465-469.
[87] B. Key, R. Bhattacharyya, M. Morcrette, V. Seznec, J.-M. Tarascon, C.P. Grey, Journal of the American Chemical Society, 131 (2009) 9239-9249.
[88] C. Brissot, M. Rosso, J.-N. Chazalviel, P. Baudry, S. Lascaud, Electrochimica acta, 43 (1998) 1569-1574.
[89] Q. Yun, Y.B. He, W. Lv, Y. Zhao, B. Li, F. Kang, Q.H. Yang, Advanced Materials, 28 (2016) 6932-6939.
[90] Y. An, H. Fei, G. Zeng, X. Xu, L. Ci, B. Xi, S. Xiong, J. Feng, Y. Qian, Nano Energy, 47 (2018) 503-511.
[91] H. Qiu, T. Tang, M. Asif, X. Huang, Y. Hou, Advanced Functional Materials, 29 (2019) 1808468.

[92] H. Liu, E. Wang, Q. Zhang, Y. Ren, X. Guo, L. Wang, G. Li, H. Yu, Energy Storage Materials, 17 (2019) 253-259.
[93] P. Zhu, Z. Wu, Y. Zhao, Scripta Materialia, 172 (2019) 119-124.
[94] S.H. Wang, Y.X. Yin, T.T. Zuo, W. Dong, J.Y. Li, J.L. Shi, C.H. Zhang, N.W. Li, C.J. Li, Y.G. Guo, Advanced Materials, 29 (2017) 1703729.
[95] C. Monroe, J. Newman, Journal of The Electrochemical Society, 150 (2003) A1377-A1384.
[96] Y. Wang, Z. Wang, D. Lei, W. Lv, Q. Zhao, B. Ni, Y. Liu, B. Li, F. Kang, Y.-B. He, ACS applied materials & interfaces, 10 (2018) 20244-20249.
[97] J.S. Wang, P. Liu, E. Sherman, M. Verbrugge, H. Tataria, Journal of Power Sources, 196 (2011) 8714-8718.
[98] Z. Du, D.L. Wood, C. Daniel, S. Kalnaus, J. Li, Journal of Applied Electrochemistry, 47 (2017) 405-415.
[99] T. Jiang, S. Zhang, X. Qiu, W. Zhu, L. Chen, Electrochemistry communications, 9 (2007) 930-934.
[100] D.H. Nam, R.H. Kim, D.W. Han, H.S. Kwon, Electrochimica Acta, 66 (2012) 126-132.
[101] X.-Y. Fan, F.-S. Ke, G.-Z. Wei, L. Huang, S.-G. Sun, Journal of Solid State Electrochemistry, 13 (2009) 1849.
[102] K.-L. Lee, J.-Y. Jung, S.-W. Lee, H.-S. Moon, J.-W. Park, Journal of power sources, 129 (2004) 270-274.
[103] C.C. Nguyen, S.-W. Song, Electrochimica Acta, 55 (2010) 3026-3033.
[104] D. Reyter, S. Rousselot, D. Mazouzi, M. Gauthier, P. Moreau, B. Lestriez, D. Guyomard, L. Roue, Journal of power sources, 239 (2013) 308-314.
[105] G.-b. Cho, Y.-m. Im, W.-r. Lee, S.-h. Lee, S.-y. Ji, G.-t. Kim, T.-h. Nam, K.-w. Kim, Thin solid films, 546 (2013) 410-413.
[106] G.-b. Cho, J.-k. Kim, S.-h. Lee, G.-t. Kim, J.-p. Noh, K.-k. Cho, K.-w. Kim, T.-h. Nam, H.-j. Ahn, Electrochimica Acta, 224 (2017) 649-659.
[107] S.-W. Kang, H.-M. Xie, W. Zhang, J.-P. Zhang, Z. Ma, R.-S. Wang, X.-L. Wu, Electrochimica Acta, 176 (2015) 604-609.
[108] J. Jiang, P. Nie, B. Ding, W. Wu, Z. Chang, Y. Wu, H. Dou, X. Zhang, ACS applied materials & interfaces, 8 (2016) 30926-30932.
[109] C. Zhang, W. Lv, G. Zhou, Z. Huang, Y. Zhang, R. Lyu, H. Wu, Q. Yun, F. Kang, Q.H. Yang, Advanced Energy Materials, 8 (2018) 1703404.
[110] H. Ye, Z.J. Zheng, H.R. Yao, S.C. Liu, T.T. Zuo, X.W. Wu, Y.X. Yin, N.W. Li, J.J. Gu, F.F. Cao, Angewandte Chemie, 131 (2019) 1106-1111.
[111] Z. Hou, Y. Yu, W. Wang, X. Zhao, Q. Di, Q. Chen, W. Chen, Y. Liu, Z. Quan, ACS applied materials & interfaces, 11 (2019) 8148-8154.
[112] L.-L. Lu, Y. Zhang, Z. Pan, H.-B. Yao, F. Zhou, S.-H. Yu, Energy Storage Materials, 9 (2017) 31-38.
[113] L. Qin, H. Xu, D. Wang, J. Zhu, J. Chen, W. Zhang, P. Zhang, Y. Zhang, W. Tian, Z. Sun, ACS applied materials & interfaces, 10 (2018) 27764-27770.
[114] J. Luo, C.C. Fang, N.L. Wu, Advanced Energy Materials, 8 (2018) 1701482.
[115] G.V. Zhuang, K. Xu, H. Yang, T.R. Jow, P.N. Ross, The Journal of Physical Chemistry B, 109 (2005) 17567-17573.
[116] T.K. Kim, W. Chen, C. Wang, Journal of Power Sources, 196 (2011) 8742-8746.
[117] I. Geoffroy, P. Willmann, K. Mesfar, B. Carre, D. Lemordant, Electrochimica acta, 45 (2000) 2019-2027.
[118] T. Liu, L. Zhao, D. Wang, J. Zhu, B. Wang, C. Guo, RSC advances, 3 (2013) 25648-25651.
[119] G.M. Veith, N.J. Dudney, Journal of The Electrochemical Society, 158 (2011) A658.
[120] S. Ohara, J. Suzuki, K. Sekine, T. Takamura, Journal of power sources, 119 (2003) 591-596.
[121] S. Ohara, J. Suzuki, K. Sekine, T. Takamura, Journal of power sources, 136 (2004) 303-306.
[122] J. Liu, Y. Li, X. Huang, R. Ding, Y. Hu, J. Jiang, L. Liao, Journal of Materials Chemistry, 19 (2009) 1859-1864.

[123] X. Xiao, P. Liu, J.S. Wang, M. Verbrugge, M.P. Balogh, Electrochemistry Communications, 13 (2011) 209-212.
[124] C. Wang, Y. Li, Y.-S. Chui, Q.-H. Wu, X. Chen, W. Zhang, Nanoscale, 5 (2013) 10599-10604.
[125] W. Mei, J. Huang, L. Zhu, Z. Ye, Y. Mai, J. Tu, Journal of Materials Chemistry, 22 (2012) 9315-9321.
[126] B. Varghese, M. Reddy, Z. Yanwu, C.S. Lit, T.C. Hoong, G. Subba Rao, B. Chowdari, A.T.S. Wee, C.T. Lim, C.-H. Sow, Chemistry of Materials, 20 (2008) 3360-3367.
[127] C.-H. Lai, K.-W. Huang, J.-H. Cheng, C.-Y. Lee, W.-F. Lee, C.-T. Huang, B.-J. Hwang, L.-J. Chen, Journal of Materials Chemistry, 19 (2009) 7277-7283.
[128] in, 2013.
[129] M.S. Jo, S. Ghosh, S.M. Jeong, Y.C. Kang, J.S. Cho, Nano-Micro Letters, 11 (2019) 3.
[130] W. Zhou, J.-L. Zheng, Y.-H. Yue, L. Guo, Nano Energy, 11 (2015) 428-435.
[131] P. Nithyadharseni, M. Reddy, B. Nalini, B. Chowdari, Materials Letters, 150 (2015) 24-27.
[132] E. Hosono, S. Fujihara, I. Honma, H. Zhou, Electrochemistry communications, 8 (2006) 284-288.
[133] Q. Sa, Y. Wang, Journal of Power Sources, 208 (2012) 46-51.
[134] S. Ni, T. Li, X. Lv, X. Yang, L. Zhang, Electrochimica Acta, 91 (2013) 267-274.
[135] Y. Fu, Z. Yang, X. Li, X. Wang, D. Liu, D. Hu, L. Qiao, D. He, Journal of Materials Chemistry A, 1 (2013) 10002-10007.
[136] X. Li, A. Dhanabalan, K. Bechtold, C. Wang, Electrochemistry Communications, 12 (2010) 1222-1225.
[137] W. Yang, G. Cheng, C. Dong, Q. Bai, X. Chen, Z. Peng, Z. Zhang, Journal of Materials Chemistry A, 2 (2014) 20022-20029.
[138] S. Ni, X. Yang, T. Li, Journal of Materials Chemistry, 22 (2012) 2395-2397.
[139] S. Ni, X. Yang, T. Li, Materials Chemistry and Physics, 132 (2012) 1103-1107.
[140] X. Wang, L. Sun, X. Hu, R.A. Susantyoko, Q. Zhang, Journal of Power Sources, 280 (2015) 393-396.
[141] H. Liu, L. Hu, Y.S. Meng, Q. Li, Nanoscale, 5 (2013) 10376-10383.
[142] B. Qu, L. Hu, Q. Li, Y. Wang, L. Chen, T. Wang, ACS applied materials & interfaces, 6 (2014) 731-736.
[143] J. Yuan, C. Chen, Y. Hao, X. Zhang, S. Gao, R. Agrawal, C. Wang, Z. Xiong, H. Yu, Y. Xie, Journal of Electroanalytical Chemistry, 787 (2017) 158-162.
[144] H. Long, T. Shi, S. Jiang, S. Xi, R. Chen, S. Liu, G. Liao, Z. Tang, Journal of Materials Chemistry A, 2 (2014) 3741-3748.
[145] Q. Li, X. Miao, C. Wang, L. Yin, Journal of Materials Chemistry A, 3 (2015) 21328-21336.
[146] T. Takamura, S. Ohara, M. Uehara, J. Suzuki, K. Sekine, Journal of Power Sources, 129 (2004) 96-100.
[147] M. Uehara, J. Suzuki, K. Tamura, K. Sekine, T. Takamura, Journal of power sources, 146 (2005) 441-444.
[148] T. Takamura, M. Uehara, J. Suzuki, K. Sekine, K. Tamura, Journal of power sources, 158 (2006) 1401-1404.
[149] S. Wang, L. Niu, C. Chen, Y. Pang, B. Liao, Z. Zhong, P. Lu, P. Li, X. Wu, J.W. Coenen, Materials Science and Engineering: A, 730 (2018) 244-261.
[150] J. Jiang, J. Liu, R. Ding, X. Ji, Y. Hu, X. Li, A. Hu, F. Wu, Z. Zhu, X. Huang, The Journal of Physical Chemistry C, 114 (2010) 929-932.
[151] Y. Li, B. Tan, Y. Wu, Nano letters, 8 (2008) 265-270.
[152] Y. Wang, H. Xia, L. Lu, J. Lin, ACS nano, 4 (2010) 1425-1432.
[153] L. Zhan, S. Wang, L.-X. Ding, Z. Li, H. Wang, Electrochimica Acta, 135 (2014) 35-41.
[154] H. Wu, M. Xu, Y. Wang, G. Zheng, Nano Research, 6 (2013) 167-173.
[155] S. Chen, M. Wang, J. Ye, J. Cai, Y. Ma, H. Zhou, L. Qi, Nano Research, 6 (2013) 243-252.
[156] L. Zhang, H.B. Wu, X.D.W. Lou, Materials Horizons, 1 (2014) 133-138.
[157] D. Cai, D. Li, L.-X. Ding, S. Wang, H. Wang, Electrochimica Acta, 192 (2016) 407-413.

[158] S. Dong, H. Wang, L. Gu, X. Zhou, Z. Liu, P. Han, Y. Wang, X. Chen, G. Cui, L. Chen, Thin Solid Films, 519 (2011) 5978-5982.
[159] Y. Tang, L. Hong, Q. Wu, J. Li, G. Hou, H. Cao, L. Wu, G. Zheng, Electrochimica Acta, 195 (2016) 27-33.
[160] S. Chen, Y. Xin, Y. Zhou, Y. Ma, H. Zhou, L. Qi, Energy & Environmental Science, 7 (2014) 1924-1930.
[161] X. Wang, B. Liu, X. Hou, Q. Wang, W. Li, D. Chen, G. Shen, Nano Research, 7 (2014) 1073-1082.
[162] L. Tian, A. Yuan, Journal of Power Sources, 192 (2009) 693-697.
[163] Z.-J. Zhang, Q.-Y. Zeng, S.-L. Chou, X.-J. Li, H.-J. Li, K. Ozawa, H.-K. Liu, J.-Z. Wang, Electrochimica Acta, 133 (2014) 570-577.
[164] M.-S. Balogun, Y. Zhu, W. Qiu, Y. Luo, Y. Huang, C. Liang, X. Lu, Y. Tong, ACS applied materials & interfaces, 7 (2015) 25991-26003.
[165] Y. Liu, R. Xiao, Y. Fang, P. Zhang, Electrochimica Acta, 211 (2016) 1041-1047.
[166] Z. Bi, M.P. Paranthaman, P.A. Menchhofer, R.R. Dehoff, C.A. Bridges, M. Chi, B. Guo, X.-G. Sun, S. Dai, Journal of Power Sources, 222 (2013) 461-466.
[167] H. Choi, H. Park, J.H. Um, W.-S. Yoon, H. Choe, Applied Surface Science, 411 (2017) 363-367.
[168] G. Lorang, M.D.C. Belo, A. Simoes, M. Ferreira, Journal of The Electrochemical Society, 141 (1994) 3347-3356.
[169] J.P. Maranchi, A.F. Hepp, P.N. Kumta, Materials Science and Engineering: B, 116 (2005) 327-340.
[170] Y. Wen, L. Shao, P. Zhao, B. Wang, G. Cao, Y. Yang, Journal of Materials Chemistry A, 5 (2017) 15752-15758.
[171] W. Fredriksson, K. Edström, Electrochimica acta, 79 (2012) 82-94.
[172] G. Zhang, K. Takashima, Y. Higo, Materials Science and Engineering: A, 426 (2006) 95-100.
[173] X. Li, L. Qiao, D. Li, X. Wang, W. Xie, D. He, Journal of Materials Chemistry A, 1 (2013) 6400-6406.
[174] D.H. Sim, X. Rui, J. Chen, H. Tan, T.M. Lim, R. Yazami, H.H. Hng, Q. Yan, RSC advances, 2 (2012) 3630-3633.
[175] C. Jacob, T. Lynch, A. Chen, J. Jian, H. Wang, Journal of power sources, 241 (2013) 410-414.
[176] L. Xue, S.V. Savilov, V.V. Lunin, H. Xia, Advanced Functional Materials, 28 (2018) 1705836.
[177] S. Shironita, N. Ihsan, K. Konakawa, K. Souma, M. Umeda, Electrochimica Acta, 295 (2019) 1052-1056.
[178] M. Park, G. Wang, H.-K. Liu, S. Dou, Electrochimica acta, 51 (2006) 5246-5249.
[179] K. Peng, J. Jie, W. Zhang, S.-T. Lee, Applied Physics Letters, 93 (2008) 033105.
[180] L. Hu, H. Wu, S.S. Hong, L. Cui, J.R. McDonough, S. Bohy, Y. Cui, Chemical Communications, 47 (2011) 367-369.
[181] J.-H. Cho, X. Li, S.T. Picraux, Journal of Power Sources, 205 (2012) 467-473.
[182] V. Aravindan, K. Jinesh, R.R. Prabhakar, V.S. Kale, S. Madhavi, Nano Energy, 2 (2013) 720-725.
[183] W. Zeng, F. Zheng, R. Li, Y. Zhan, Y. Li, J. Liu, Nanoscale, 4 (2012) 2760-2765.
[184] Y.-Q. Chu, Z.-W. Fu, Q.-Z. Qin, Electrochimica Acta, 49 (2004) 4915-4921.
[185] H. Yue, F. Li, Z. Yang, J. Tang, X. Li, D. He, Materials Letters, 120 (2014) 39-42.
[186] X. Xu, J. Liu, R. Hu, J. Liu, L. Ouyang, M. Zhu, Chemistry–A European Journal, 23 (2017) 5198-5204.
[187] G.-P. Kim, S. Park, I. Nam, J. Park, J. Yi, Journal of power sources, 237 (2013) 172-177.
[188] G.-P. Kim, I. Nam, N.D. Kim, J. Park, S. Park, J. Yi, Electrochemistry communications, 22 (2012) 93-96.
[189] H.-C. Liu, S.-K. Yen, Journal of Power Sources, 166 (2007) 478-484.
[190] M. Laurenti, N. Garino, S. Porro, M. Fontana, C. Gerbaldi, Journal of Alloys and Compounds, 640 (2015) 321-326.
[191] V. Channu, R. Bobba, R. Holze, Colloids and Surfaces A: Physicochemical and Engineering Aspects, 436 (2013) 245-251.
[192] K. Feng, H.W. Park, X. Wang, D.U. Lee, Z. Chen, Electrochimica Acta, 139 (2014) 145-151.

[193] Q. Chu, B. Yang, W. Wang, W. Tong, X. Wang, X. Liu, J. Chen, ChemistrySelect, 1 (2016) 5569-5573.
[194] H.-Y. Cheng, P.-Y. Cheng, X.-F. Chuah, C.-L. Huang, C.-T. Hsieh, J. Yu, C.-H. Lin, S.-Y. Lu, Chemical Engineering Journal, 374 (2019) 201-210.
[195] E. Pomerantseva, K. Gerasopoulos, X. Chen, G. Rubloff, R. Ghodssi, Journal of Power Sources, 206 (2012) 282-287.
[196] X. Li, D. Li, Z. Wei, X. Shang, D. He, Electrochimica Acta, 121 (2014) 415-420.
[197] S.K. Martha, N.J. Dudney, J.O. Kiggans, J. Nanda, Journal of The Electrochemical Society, 159 (2012) A1652.
[198] S. Flandrois, B. Simon, Carbon, 37 (1999) 165-180.
[199] F. Barbir, PEM Fuel Cells: Theory and Practice, (2005) 73-113.
[200] J.W. Choi, L. Hu, L. Cui, J.R. McDonough, Y. Cui, Journal of Power Sources, 195 (2010) 8311-8316.
[201] J. Guo, A. Sun, C. Wang, Electrochemistry communications, 12 (2010) 981-984.
[202] M. Shafiei, A.T. Alpas, Journal of Power Sources, 196 (2011) 7771-7778.
[203] Y. Shi, B. Wang, Progress in Natural Science: Materials International, 24 (2014) 56-60.
[204] G. Zhou, F. Li, H.-M. Cheng, Energy & Environmental Science, 7 (2014) 1307-1338.
[205] H. Lu, J. Hagberg, G. Lindbergh, A. Cornell, Nano Energy, 39 (2017) 140-150.
[206] H. Lu, J. Hagberg, G. Lindbergh, A. Cornell, Batteries, 4 (2018) 17.
[207] R.A. Susantyoko, X. Wang, Q. Xiao, E. Fitzgerald, Q. Zhang, Carbon, 68 (2014) 619-627.
[208] C.-H. Hsu, H.-H. Lin, Y.-H. Liu, H.-P. Lin, New Journal of Chemistry, 42 (2018) 9058-9064.
[209] H. Wolf, Z. Pajkic, T. Gerdes, M. Willert-Porada, Journal of Power Sources, 190 (2009) 157-161.
[210] L.-L. Zhang, Z. Li, X.-L. Yang, X.-K. Ding, Y.-X. Zhou, H.-B. Sun, H.-C. Tao, L.-Y. Xiong, Y.-H. Huang, Nano Energy, 34 (2017) 111-119.
[211] S. Chu, Y. Zhong, R. Cai, Z. Zhang, S. Wei, Z. Shao, Small, 12 (2016) 6724-6734.
[212] Z. Liu, S. Bai, B. Liu, P. Guo, M. Lv, D. Liu, D. He, Journal of Materials Chemistry A, 5 (2017) 13168-13175.
[213] J. Guo, X. Chen, C. Wang, Journal of Materials Chemistry, 20 (2010) 5035-5040.
[214] K. Fu, O. Yildiz, H. Bhanushali, Y. Wang, K. Stano, L. Xue, X. Zhang, P.D. Bradford, Advanced Materials, 25 (2013) 5109-5114.
[215] J.W. Hu, Z.P. Wu, S.W. Zhong, W.B. Zhang, S. Suresh, A. Mehta, N. Koratkar, Carbon, 87 (2015) 292-298.
[216] A.M. Gaikwad, B.V. Khau, G. Davies, B. Hertzberg, D.A. Steingart, A.C. Arias, Advanced Energy Materials, 5 (2015) 1401389.
[217] L. Hu, F. La Mantia, H. Wu, X. Xie, J. McDonough, M. Pasta, Y. Cui, Advanced Energy Materials, 1 (2011) 1012-1017.
[218] S.-J. Kim, M.-C. Kim, S.-B. Han, G.-H. Lee, H.-S. Choe, S.-H. Moon, D.-H. Kwak, S. Hong, K.-W. Park, Journal of Industrial and Engineering Chemistry, 49 (2017) 105-111.
[219] K. Lin, X. Qin, M. Liu, X. Xu, G. Liang, J. Wu, F. Kang, G. Chen, B. Li, Advanced Functional Materials, 29 (2019) 1903229.
[220] D. Chao, X. Xia, J. Liu, Z. Fan, C.F. Ng, J. Lin, H. Zhang, Z.X. Shen, H.J. Fan, Advanced materials, 26 (2014) 5794-5800.
[221] R. Mo, D. Rooney, K. Sun, H.Y. Yang, Nature communications, 8 (2017) 1-9.
[222] J. He, Q. Li, Y. Chen, C. Xu, K. Zhou, X. Wang, W. Zhang, Y. Li, Carbon, 114 (2017) 111-116.
[223] Y. Tang, J. Sha, N. Wang, R. Zhang, L. Ma, C. Shi, E. Liu, N. Zhao, Carbon, 158 (2020) 536-544.
[224] M.A. Peña-Guerrero, C. Leitherer, S. de Mink, A. Wofford, L. Kewley, The Astrophysical Journal, 847 (2017) 107.
[225] M. Henckens, P. Driessen, E. Worrell, Resources, Conservation and recycling, 93 (2014) 1-8.
[226] T. Or, S.W. Gourley, K. Kaliyappan, A. Yu, Z. Chen, Carbon Energy, (2020).
[227] J. Marshall, D. Gastol, R. Sommerville, B. Middleton, V. Goodship, E. Kendrick, Metals, 10 (2020) 773.
[228] H. Wang, J. Liu, X. Bai, S. Wang, D. Yang, Y. Fu, Y. He, Waste Management, 91 (2019) 89-98.

[229] A. Savvatimskiy, Carbon, 43 (2005) 1115-1142.
[230] G.-F. Yang, S.-K. Joo, Electrochimica Acta, 170 (2015) 263-268.
[231] D.J. Noelle, M. Wang, Y. Qiao, Journal of Power Sources, 399 (2018) 125-132.
[232] S. Poetz, B. Fuchsbichler, M. Schmuck, S. Koller, Journal of applied electrochemistry, 44 (2014) 989-994.